

3-9-2016

Clearance Analysis of 3D Printed Assemblies Using Fused Filament Extrusion

Kshitij Luthria
kjl6993@rit.edu

Follow this and additional works at: <http://scholarworks.rit.edu/theses>

Recommended Citation

Luthria, Kshitij, "Clearance Analysis of 3D Printed Assemblies Using Fused Filament Extrusion" (2016). Thesis. Rochester Institute of Technology. Accessed from

This Thesis is brought to you for free and open access by the Thesis/Dissertation Collections at RIT Scholar Works. It has been accepted for inclusion in Theses by an authorized administrator of RIT Scholar Works. For more information, please contact ritscholarworks@rit.edu.

ROCHESTER INSTITUTE OF TECHNOLOGY

**CLEARANCE ANALYSIS OF 3D
PRINTED ASSEMBLIES USING
FUSED FILAMENT EXTRUSION**

Kshitij Luthria

Thesis submitted to the Faculty of the
Rochester Institute of Technology

In partial fulfillment of the requirements for the degree of
Master of Science in Industrial Engineering

**Rochester Institute of Technology
Rochester, NY
March 9, 2016**

**DEPARTMENT INDUSTRIAL ENGINEERING
KATE GLEASON COLLEGE OF ENGINEERING
ROCHESTER INSTITUTE OF TECHNOLOGY
ROCHESTER, NEW YORK
CERTIFICATE OF APPROVAL**

M.S. DEGREE THESIS

**The M.S. Degree Thesis of Kshitij Luthria
has been examined and approved by the
thesis committee as satisfactory for the
thesis requirement for the
Master of Science degree**

Approved by:

Dr. Denis Cormier, Thesis Advisor

Dr. Ronald Aman, Committee Member

Abstract

3D Printing technologies have been around for the better part of 30 years now, and researchers today have a reasonably good understanding of how the different processes work. A focus for the next era of 3D printing will likely be to gain a deeper understanding of how these processes can be used in unique applications. One such unique application that can potentially change the way conventional manufacturing works involves 3D printing of assemblies. By printing assemblies ‘in-situ’, multiple assembly steps can be by-passed, thus increasing efficiency and decreasing costs. This research specifically seeks to develop an understanding of how clearances between mating surfaces in 3D printed assembly components should be designed based on the orientations of the surfaces and the 3D printing process used.

A design of experiments (DOE) approach was used to identify significant process parameters affecting the clearances obtained between mating surfaces in a 3D printed assembly. Factors such as the surface angle, CAD clearance between mating surfaces, and 3D printer layer thickness were all considered. The experiments were carried out on a MakerBot Replicator 2X machine, although the experimental methodology applies to other processes as well. The samples obtained were examined using a Hirox 7700 digital microscope to quantify differences between the CAD model design clearances and 3D printed clearances between mating surfaces in the assembly. The optimal ranges for experimental factors were thus derived.

Based on results of the designed experiments, pin-hole assembly test samples were printed using the optimal range of parameter values. An unconventional method was then applied using a cylindrical pin-polygon assembly, which revealed that this method was more accurate in obtaining the desired clearances in a 3D printed moving assembly.

Acknowledgements

I wish to express my most sincere gratitude to my advisor Dr. Denis Cormier for giving me the opportunity to work on this research and for his continuous support, motivation and guidance. I feel fortunate to learn from his breadth of knowledge and valuable research literature in the field of additive manufacturing. I would also like to thank Dr. Ron Aman for his insights and guidance during the course of my thesis.

Additionally, I would like to thank John Bonzo & Chaitanya Mahajan for their kind help and suggestions. Sincere thanks to the entire faculty in the Industrial & Systems Engineering department for their help and support as always.

I would like to extend my gratitude to my fellow Industrial engineering graduate students, roommates and to all who helped me throughout my master's journey. A special thanks my girlfriend Laura Vas for being with me through thick and thin.

Finally, I want to thank my parents and sister for their love and support, their spiritual point of view in life has helped me get through tough times with ease.

Table of Contents

1	Introduction	1
1.1	Fused Filament Extrusion.....	3
2	Literature Review	5
2.1	Research Objectives.....	8
3	Research Methodology	9
3.1	Preliminary Experimentation: Analysis of slot width at various angles of printing	9
3.1.1	Methods and Material	10
3.1.2	Evaluation and Measurement.....	11
3.1.3	Preliminary Results	15
3.1.4	Conclusions from the Feasibility test.....	17
3.2	Design of Experiments	17
3.2.1	Experimental Set-up.....	18
3.2.2	Evaluation and Measurement.....	21
3.2.3	Analysis of Results from the Design of Experiments.....	23
3.2.4	Conclusions from the Design of Experiments	28
4	3D Printing a moving assembly.....	29
4.1	3D Printed Hole Methodology	29
4.2	3D Printed Hole Results	30
4.3	3D Printed Hole Conclusions.....	33
4.4	3D Printed Polygonal Hole-Pin Features.....	33
5	Conclusions and Recommendations for Future Research	40
5.1	Summary	40
5.2	Recommendations for Future Work	41
6	References	43
7	Appendix: Micrographs for Design of Experiments	45

Table of Figures

Figure 1: Models of manufacturing practice.....	2
Figure 2:Slicing in a STL model[6]	3
Figure 3: FFE process.....	4
Figure 4: Staircase effect in FDM: (a) Original CAD geometry; (b) Faceted STL file of CAD geometry; (c) Representation of 3D printed part with stair-stepping effect due to printed layers.	5
Figure 5:1mm Slot width analysis	Figure 6: 0.5mm Slot width analysis.....
Figure 7: Measurements (in mm) taken for each region of the slot.....	12
Figure 8: Measurements within each region of the slot.....	12
Figure 9: Interval plot of slot width error for specified slot width of 1mm	16
Figure 10: Interval plot of slot width error for specified slot width of 0.5mm	17
Figure 11: Print settings for design of experiment	18
Figure 12: Whole plot design	19
Figure 13: Slot width and slot orientation	20
Figure 14: Layer Thickness	20
Figure 15: Slot width measurements taken at 4 points of the slot	21
Figure 16: Enlarged view of measurements taken for DOE.....	21
Figure 17: Row number vs residuals for error in slot width	24
Figure 18: Normality plot for error in slot width	24
Figure 19: Interaction plot for error in slot width.....	25
Figure 20: (a) Surface plot slot width error w.r.t slot angle (b) Surface plot slot width error w.r.t slot width (c) Surface plot slot width error w.r.t layer thickness	27
Figure 21: Diagrammatic representation of the drooping phenomenon in down facing surfaces	28
Figure 22: 3D printed holes samples.....	29
Figure 23: Relative error measured for 3D printed hole	33
Figure 24: (a) Conventional approach for a pin-hole assembly; (b) Unconventional approach for a pin-hole assembly where hexagonal hole is at a 30° to the build plate; (c) Unconventional approach for a pin-hole assembly where hexagonal hole is at a parallel to the build plate.....	35
Figure 25: Print preview in of the build platform showing assemblies in four different orientations along with support structures	36
Figure 26: Moving cylindrical pin-hexagon hole assembly	37
Figure 27: Fused cylindrical pin- cylindrical hole assembly	38
Figure 28: Whole Plot 1.....	46
Figure 29: Whole Plot 2.....	47
Figure 30: Whole Plot 3.....	48
Figure 31: Whole Plot 4.....	49
Figure 32: Whole Plot 5.....	50
Figure 33: Whole Plot 6.....	51
Figure 34: Whole Plot 7.....	52
Figure 35: Whole Plot 8.....	53
Figure 36: Whole Plot 9.....	54

List of Tables

Table 1: Print settings for analysis of slot width at various angles of printing	11
Table 2: Measurement data (in mm) for 1mm slot width	Error! Bookmark not defined.
Table 3: Measurement data (in mm) for 0.5mm slot width (mm units)	14
Table 4: DOE factors and levels.....	20
Table 5: Design table and data for design of experiment.....	22
Table 6: Summary of fit and parameter Estimates.....	23
Table 7 : Measured hole diameters for a nominal (specified) hole diameter of 8 mm printed at different orientations w.r.t the X-Y build plane along with the calculated relative error	30
Table 8: Measured hole diameters for a nominal (specified) hole diameter of 10 mm printed at different orientations w.r.t the X-Y build plane along with the calculated relative error	31
Table 9: Measured hole diameters for a nominal (specified) hole diameter of 12 mm printed at different orientations w.r.t the X-Y build plane along with the calculated relative error	31
Table 10: Measured hole diameters for a nominal (specified) hole diameter of 14 mm printed at different orientations w.r.t the X-Y build plane along with the calculated relative error	32
Table 11: Dimensions used to print the hexagonal hole-cylindrical pin validation assembly.....	39
Table 12: Dimensions used to print the cylindrical hole-cylindrical pin validation assembly	39

1 Introduction

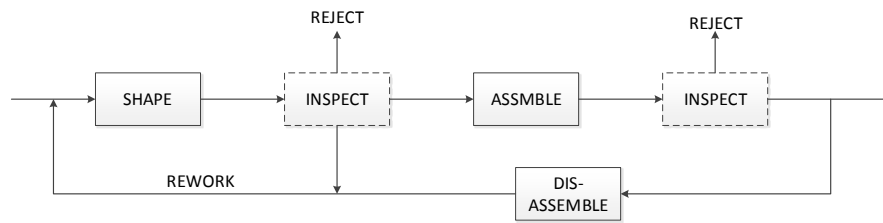
3D printing technologies have asserted their presence in the manufacturing world over the past decade and have the ability to potentially replace some conventional manufacturing processes in the years to come. Though the technology has grown leaps and bounds, there are still several drawbacks limiting its use for rapid manufacturing [1]. That being said, there is a great amount of research being carried out to help this technology become a primary manufacturing process in factories across the world.

Much of modern manufacturing relies on interchangeability and standardization [2]. This method works perfectly well in a mass production environment, where lot sizes range from hundreds of thousands to millions. However, consider a situation where a customer wants to place a large order in which every piece is unique. Conventional manufacturing methods will fail as the manufacturer will have to develop special tooling for each part. The economies of scale do not add up, resulting in an unprofitable business model.

Conventional assembly lines are designed as a series of stations where new components are added to the product at every station (Figure 1 a). Consider a situation where a change is to be made at Station 1 which alters the outer shape of the product. This change will now affect the next station and may even affect the tooling at all other stations downstream, hence this method is rigid and doesn't allow changes to the process freely.

Subsequently, recent advancements in the field of additive manufacturing can help overcome the aforementioned problems related to manufacturing. Recent technologies make it possible to manufacture entire assemblies incrementally, with no subsequent assembly operations required (Figure 1 b). 3D printing technologies are capable of fabricating parts with complex internal geometry and multiple materials. Additionally, these processes' build parts are encapsulated in a sacrificial support structure, which makes it possible to fabricate multiple-part assemblies with bearing, mating and fitting surfaces in-situ. Designers

have the option of directly specifying the geometry of gaps and clearances with explicit tolerance assignments.[2]



(a) Conventional Manufacturing and Assembly Process



(b) Additive Manufacturing

Figure 1: Models of manufacturing practice

3D printing provides us with the freedom to produce parts having such geometric complexities that cannot be produced by other manufacturing processes. Furthermore, some of these complex geometries are relatively difficult to assemble via conventional methods. By using 3D printing, we can not only produce parts with geometric complexities but we can produce these parts as fully functional assemblies. This method provides for a wide variety of practical applications especially in the field of medicine, where part sizes are small and have an extremely complex geometry, these parts also require a great deal of precision which can be provided by 3D printing.

While there are clear advantages of using this technology, there are a lot of questions that are still unanswered and need to be studied in greater detail in order for this application of the technology to gain widespread acceptance, such as, how to print parts with a small gap between mating surfaces that don't fuse together? How large should the gap be? Is the gap to be provided process and machine specific? Is the gap to be provided orientation specific? This thesis aims to answer some of these questions and develop strategies to help overcome the drawbacks of the conventional approaches used to 3D print assemblies.

1.1 Fused Filament Extrusion

Fused Filament Extrusion (FFE) is the most common and widely used additive manufacturing process available today [3]. The process was developed in the late 1980's and was patented by Stratasys in 1989 [4]. With the expiration of the patent and increased interest in the technology, there has been a surge of companies and crowd sourcing projects which utilize the FFE process or a variation of it to manufacture products.

The process starts with creation of a 3D CAD model of the object to be printed. The CAD model is converted into the STL file format. The STL model is “mathematically sliced by intersecting it with horizontal planes, each slice represents a cross-section data for the part and the layer thickness is defined as the distance between the planes” [5]. Using the section data, the software generates tool paths which drive the extrusion head. The toolpath data is then downloaded to the FFE machine to be used.

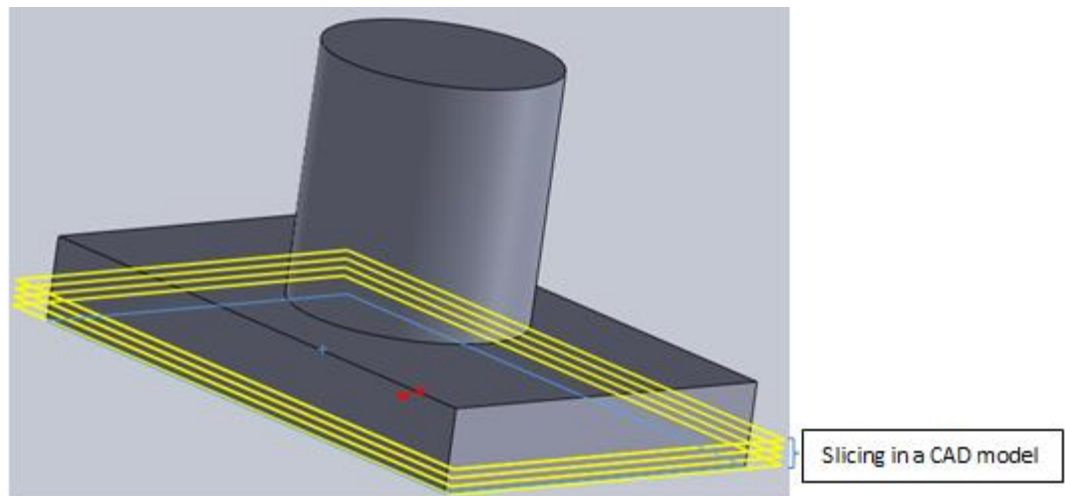


Figure 2: Slicing in a CAD model

A thermoplastic filament is fed into a heated nozzle whose temperature exceeds the melting point of the feedstock. The soft polymer is extruded through a nozzle of a given diameter. An X-Y stage with a belt and pulley mechanism moves the nozzle over the prescribed tool path while the material is extruded onto a heated build plate, thus printing the first layer of material. Once a layer is printed, the build plate lowers by an amount equal to the set layer height, thus enabling the next layer to be printed on top of the previous

printed layer (Figure 3). The movement of the build plate in the vertical direction (Z axis) and the movement of the nozzle in the horizontal (X-Y axis) is controlled using a microprocessor [4].

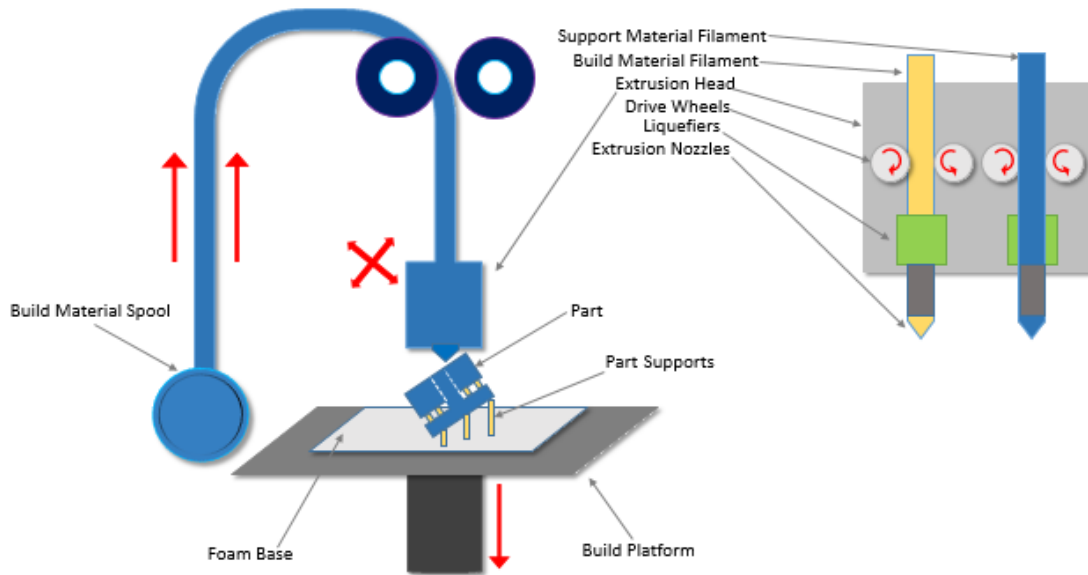


Figure 3: FFE process

The FFE process allows the user to print support structures beneath down-facing surfaces as well. A support structure is formed by depositing material which will ultimately be under suspended portions of the object being formed. As the part is being printed one layer at a time, the overhanging portions or portions of the part suspended against gravity are held in place by these support structures. They prevent the material from falling into undercuts, hollow features or onto the base [6]. Following completion of the build, the support structure is removed by either breaking it away, or dissolving it in a suitable solution [7].

The amount of support structure required will vary according to the build orientation of the part with respect to the build plate. Parts being printed parallel to the build plate will require less support material as a lesser portion of the part will be suspended under gravity, while parts which are at an angle to the build plate will require more support material to hold the part in place. The use of support material also has an effect on the surface finish of the part as the support structure minimizes the sagging of the part which is suspended against gravity.

2 Literature Review

The FFE process builds parts using a layering process based upon the STL file format. The STL file format approximates the surfaces of an object by a set of facets (triangles) as illustrated in Figure 4(b). When this part is sliced into the layers to be printed, the well-known staircase effect results as illustrated in Figure 4(c). According to Arni and Gupta [8], the extent of the staircase effect depends on the layer thickness and slope of the surface relative to the build plane. As shown in Figure 4, different orientations of the shaded face with respect to the build plane produce different degrees of the staircase effect. Whether a part can be produced with an acceptable accuracy and surface finish therefore depends on the build orientation. In the case where an assembly of parts are 3D printed, the accuracy and surface finish of opposing faces in the assembly components are critical in determining whether or not the printed assembly will function properly.

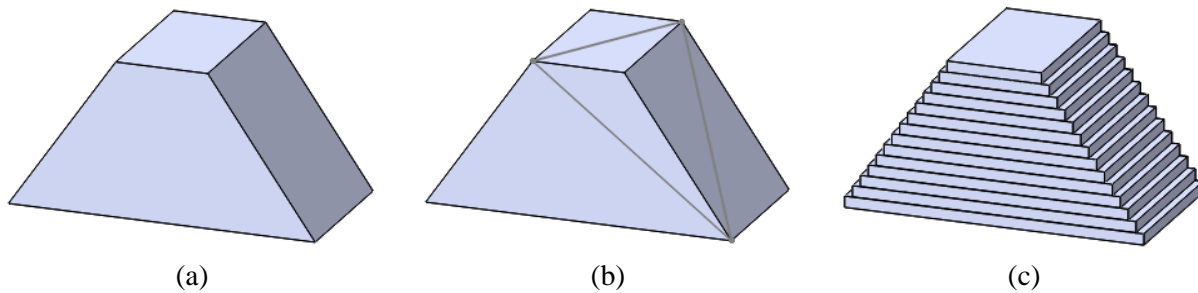


Figure 4: Staircase effect in FDM: (a) Original CAD geometry; (b) Faceted STL file of CAD geometry; (c) Representation of 3D printed part with stair-stepping effect due to printed layers.

Although relatively little research has been published on the subject of 3D printed assemblies, there is a wealth of published research on accuracy and surface finish. Paul *et al.* studied the effect of build orientation on cylindricity error using an analytical approach and by simulating the manufacturing surface based on the CAD and STL models of the part. The concept of a feasibility range for cylindricity tolerance was introduced, and the acceptable ranges of the orientation angles between the cylinder axis and build vector were also calculated.

The main contributions of the approach presented by the authors is a graphical method to identify optimal orientation zones that satisfy the cylindricity tolerance for a part with multiple cylindrical features. This

contribution provides designers with a technique to tweak the tolerance callouts on the cylindrical features depending upon the process parameters of the RM process [9].

Ippolito *et al.* investigated the development, manufacture and testing of a benchmark to investigate dimensional accuracy and surface finish of five rapid prototyping techniques: stereolithography (SLA), solid ground curing (SGC), selective laser sintering (SLS), fused deposition modeling (FDM) and laminated object manufacturing (LOM). The study showed that surface finish was the crucial feature in many cases. This was often corrected by means of manual operations to the detriment of precision, production times, and cost. Hence the final result is greatly dependent on the skillfulness of the operator. The authors further specify the need for advancement from the present stage of empiricism to a fuller knowledge of the links between process parameters and the geometrical and physical features of the part produced [10].

The influence of FDM machining parameters on surface finish of ABS parts was studied by Galantucci *et al.* The surface finish of the products after the modification of extrusion parameters was measured and processed through designed experiments. The results indicated that the process parameters had an effect on the R_a values. They identified slice height and raster width as important parameters, while the tip diameter had little importance. The authors proposed a post-processing treatment that yielded a significant improvement of the R_a [11].

The effect of part orientation on cylindricity and flatness errors was analyzed by Paul and Anand [12]. The authors' intent was to manufacture precision parts through optimal part orientation of 3D printed parts with minimal support structures. The authors point out that one of the main contributors to the energy and material consumption in layered manufacturing processes are the support structures. They developed a voxel based algorithm to determine the optimal part orientation for minimum support structure volume. They were able to minimize the support structures while still satisfying the tolerance callouts on critical features. The authors also state that the areas requiring support structures tend to have poor surface roughness, and the production of error free high precision parts with minimal material utilization will push layered manufacturing from a niche to a more widespread industry accepted manufacturing process.

Relvas et al. identified that there is a lack of published data related to rapid prototyping processes and feature accuracy. They conducted their research to minimize this gap and provide much needed accuracy in terms of dimensional and geometric information. The research showed that there are few benefits to generating STL files with extremely high resolution. This kind of refinement would not necessarily result in obtaining more accurate models. The research further showed that despite technological advances in processes such as FFE and binder jetting, the accuracy of these processes can exceed the $\pm 0.300\text{mm}$ range. The researchers conclude that these technologies may be acceptable for concept modeling, but caution is needed for parts with certain functional requirements [13].

A surface roughness visualization model was developed by Campbell et al. The basis of this research was that surface roughness of Rapid Prototype (RP) models will vary predictably across their total surface area. The challenge to the RP user is to minimize the adverse effects of surface roughness through careful orientation of the model during production. The authors developed a test geometry part; this part was printed in a single setting so that surface roughness measurements could easily be taken for surface orientations ranging from 2° to 180° at intervals of 2° . For the FFE process, the results showed that surface roughness was predictable for surface orientations between 45° and 180° . However, on upward facing surfaces that were within 45° of horizontal, there was considerable variation in measured surface roughness. The authors concluded that stair stepping was not the main factor in determining surface roughness. They also suggest that researchers should look at other ways of improving surface roughness other than reducing layer thickness [14].

Krolczyk et al. investigated the surface integrity of both turned machined parts and FFE parts. Surface analysis was made using novel metrology methods: auto correlation and gradient distribution. An Infinite Focus Measurement Machine (IFM) was used for the surface texture analysis. Surfaces obtained by FFE technology were composed of high peaks providing a small initial contact area and thus high areas of contact stress when the surface was contacted. The authors observed smooth gradients on turned surfaces, while FFE surfaces were characterized by steep gradients [15].

2.1 Research Objectives

Limited research is available on many RP processes. It has been found that questions pertaining to accuracy, surface quality and strength are often avoided in case studies and equipment manufacturer's websites. At most, this information is stated in the vaguest form [16]. There are many books available which cover the basics of RP technologies. However, many of the important details pertaining to RP are only available in papers, patents, or proprietary corporate documents. Therefore, standardized methods for evaluating the accuracy, surface quality, and mechanical properties of RP parts have not been sufficiently developed [17]. Literature on the subject shows that the accuracy of RP parts can be very important. However, the process of determining the dimensional accuracy of parts produced by various RP systems is not a simple task.

Tolerance and precision are obviously important factors when choosing an RP process. 3DP is continuing to improve, but it still is unable to hold the accuracy that CNC machining can [18]. In order to exploit the strengths of 3DP, process capability profiles that include characteristics such as accuracy, surface finish, strength, elongation, build times and cost must be determined [16]. Vayre et al. state the need for greater study in the field with respect to 3D printing of assemblies in their paper *Designing for Additive Manufacturing* [19].

The literature shows that researchers have worked on improving the properties of 3D printed parts relating to surface finish and dimensional accuracy. The available literature on surface finish and dimensional accuracy is very specific to printing individual parts, while very little research has been done to study these parameters on 3D printed assemblies. Hence, there exists a need to study the surface finish and dimensional accuracy that is needed to successfully 3D print functional assemblies of parts. Furthermore, virtually nothing has been published on determining the minimum separation distance between mating surfaces in an assembly. This research focuses developing a standardized method to determine the ideal part orientation and separation distance (gap) between mating surfaces.

3 Research Methodology

In the previous chapter, 3D printing of assemblies was found to be a promising application of the technology. However, very limited research has been performed that is specific to the printing of assemblies. To build upon the existing research and gain a deeper understanding of the clearances required to successfully 3D print a functional assembly, the research objectives presented here can be summarized as follows:

1. Experimentally determine the magnitude of error between specified CAD model dimensions and the corresponding measured dimensions in 3D printed assemblies.
2. Identify the process parameters (experimental factors) that have the greatest influence on dimensional errors in 3D printed assemblies.
3. Use lessons learned from the experimental studies to propose build strategies for successful 3D printing of component assemblies.
4. Demonstrate a fully functional moving 3D printed assembly whose geometry has been modified using the build strategies to compensate for dimensional errors.

3.1 Preliminary Experimentation: Analysis of slot width at various angles of printing

In order to determine the magnitude of error between the specified CAD model dimensions of a clearance slot between mating surfaces in an assembly and the corresponding measured clearance slot dimensions in a 3D printed sample, a feasibility test was conducted. The aim of this test was to determine the clearance slot width dimension at different print orientations and to compare the measured dimensions with the specified CAD model dimensions.

3.1.1 Methods and Material

Two solid models, having slot widths of 1 mm and 0.5 mm respectively were designed using the SolidWorks CAD package. These models consisted of rectangular 75 mm x 25 mm x 10 mm blocks. Two blocks were created (Figure 5 & 6), each with a set of slots at different angles with respect to the horizontal plane. These slots were designed to serve as simulated gaps between pairs of mating surfaces in a printed assembly. Two blocks having slot widths of 1mm and 0.5 mm, respectively, were created. This study aimed to find a correlation between actual 3D printed error in slot width from the specified CAD slot width and the orientation of the slot. To analyze this relationship, it was decided to take a range of angles between the 0° (horizontal slot orientation) and 90° (vertical slot orientation). The angles chosen for the study were 0°, 15°, 30°, 45°, 60°, 75° and 90°. Figures 5 and 6 show the wide and narrow gap CAD models respectively. The rationale behind taking a range of angles between 0° and 90° was to measure the actual slot width at these angles and to compare them with the specified CAD model slot width in order to determine the possibility of spotting any trends in the printing process.

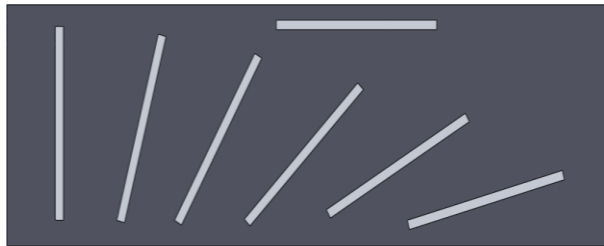


Figure 5: 1mm Slot width analysis

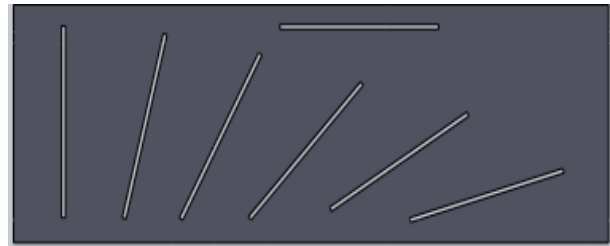


Figure 6: 0.5mm Slot width analysis

The SolidWorks CAD models were saved in the STL file format prior to being loaded into the Makerware software 3.5.0.39 and run on MakerBot Replicator 2X 3D printers. The default print parameters for ABS plastic were chosen as shown in Table 1. The models were printed on a MakerBot Replicator 2x 3D printer using 1.75 mm diameter black ABS filament (Makerbot Inc., Brooklyn, NY).

Table 1: Print settings for analysis of slot width at various angles of printing

PRINT SETTINGS		
Left Extruder: No Filament	Quality:	Right Extruder: MakerBot ABS
Resolution: Standard	Infill: 20%	Raft: Right Extruder
Profile: Standard	Number of Shells: 3	Supports: Off
Slicer: Makerbot Slicer	Layer Height: 0.1 mm	
	Temperature:	
	Left Extruder: 90 °C	
	Right Extruder: 230 °C	
	Build Plate: 110 °C	
	Speed:	
	Speed while Extruding: 90 mm/s	
	Speed while Extruding: 150 mm/s	

3.1.2 Evaluation and Measurement

Once the models were printed, the slot widths were measured using a Hirox 7700 digital microscope. The microscope's integrated software measurement tool was used to analyze the 3D printed gap width in relation to the nominal gap width from the CAD model. Low magnification images were obtained to provide the largest possible field of view.

For every slot printed nine width measurements were taken along the length (3 in the top third of the slot, 3 in the middle third of the slot and 3 in the bottom third of the slot) as shown in Figures 7 and 8. As shown in Figure 8, the expected peaks and valleys associated with the stair stepping effect are quite evident. For purposes of determining suitable assembly clearances, the minimum gap widths between the peaks of opposing faces were measured. The numerical values shown in Figure 7 correspond to the 3 separate measurements that were taken for each region of the slot (top, middle, and bottom), and the numerical values in Figure 8 correspond to the 3 measurements taken within each region. This data was collected for the 1 mm gap width sample as well as the 0.5 mm gap width sample. A total of 63 slot width data points (7 slots x 9 measurements per slot) were obtained for each of the above printed samples as shown in Tables 2 and 3.




90		0.866
		0.851
		0.845
		0.789
		0.778
		0.845
		0.794
		0.747
		0.758

Figure 7: Measurements (in mm) taken for each region of the slot

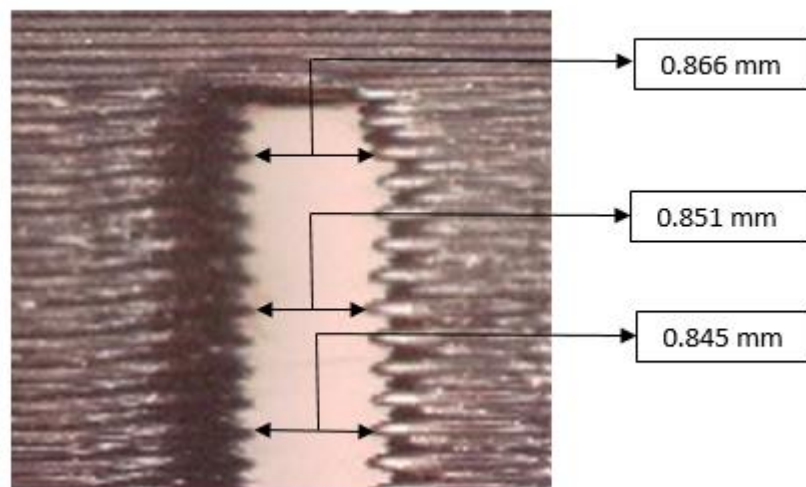


Figure 8: Measurements within each region of the slot

Table 2: Measurement data (in mm) for 1mm slot width



































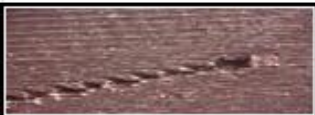







1mm					
90		0.866	75		0.765
		0.851			0.813
		0.845			0.784
		0.789			0.781
		0.778			0.724
		0.845			0.725
		0.794			0.778
		0.747			0.75
		0.758			0.785
60		0.888	45		1.025
		0.911			0.893
		0.931			0.934
		0.96			0.948
		0.98			0.85
		1.056			0.799
		1.051			0.888
		0.924			0.854
		0.714			0.77
30		0.653	15		0.468
		0.642			0.306
		0.976			0.356
		1.106			0.494
		0.876			0.321
		0.876			0.532
		0.994			0.544
		0.964			0.459
		0.745			0.402
0		0.629			
		0.506			
		0.485			
		0.289			
		0.397			
		0.521			
		0.294			
		0.532			
		0.665			

Table 3: Measurement data (in mm) for 0.5mm slot width (mm units)

0.5mm					
90		0.329	75		0.317
		0.368			0.507
		0.375			0.521
		0.368			0.436
		0.356			0.539
		0.379			0.412
		0.321			0.363
		0.313			0.352
		0.298			0.311
60		0.356	45		0.595
		0.435			0.666
		0.655			0.568
		0.737			0.577
		0.671			0.697
		0.674			0.52
		0.733			0.6
		0.536			0.552
		0.385			0.407
30		0.635	15		0.14
		0.263			0.159
		0.558			0.184
		0.185			0.196
		0.331			0.146
		0.371			0.132
		0.505			0.233
		0.608			0.148
		0.378			0.098
0		0.41			
		0.344			
		0.399			
		0			
		0			
		0			
		0.286			
		0.224			
		0.124			

3.1.3 Preliminary Results

The slot width data obtained using the Hirox microscope was entered into Minitab and analyzed for the presence of trends which would help determine the co-relation between the slot angle and the error obtained between the specified CAD slot width and slot width measured from the printed samples.

An interval plot was created for the data obtained from the 1mm slot width sample using Minitab. The interval plot (Figure 9) shows the mean and 95% confidence interval of the slot width error at every angle of print. The slot width error was calculated by using the formula:

$$\begin{aligned} \text{Slot Width Error (mm)} \\ = \text{Specified CAD Slot Width Dimension} - \text{Measured Slot Width Dimension} \end{aligned} \quad (1)$$

It was observed that the average slot width error was very high for orientations of 0° and 15°. As the slot orientation angle was increased, it was observed that the average error decreased till about 60°, providing the lowest error at 60° with a mean of 0.065 mm. As the slot orientation was further increased, it was observed that the slot width error increased at 75° and 90° but was lower than the error observed between 0° and 15°. It was also observed that though the error was high for lower angles they also had lower variance, as the orientation was increased, it was observed that the highest variance between measurements occurred at around 30° after which the variance reduced with increase in orientation reaching a minimum value at 75°.

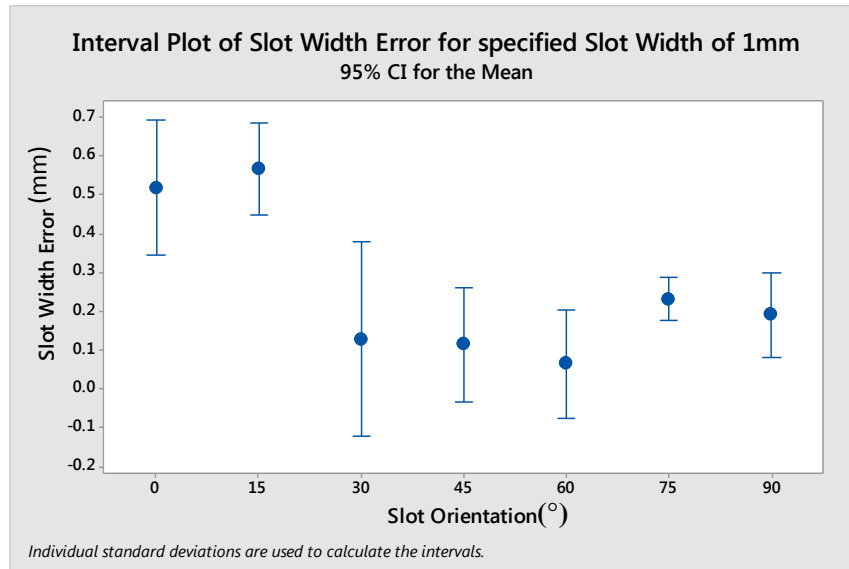


Figure 9: Interval plot of slot width error for specified slot width of 1mm

An interval plot was created for the data obtained from the 0.5 mm slot width sample using Minitab. The interval plot (Figure 10) shows the mean and 95% confidence interval of the slot width error at every angle of print. It was observed that the average slot width error was very high for slot orientations of 0° and 15°. As the slot orientation was increased, it was observed that the error reduced till about 60°, providing the lowest error at 60° with a mean of -0.075 mm. As the slot orientation was further increased, it was observed that the slot width error increased at 75° and 90° but was lower than the error observed between 0° and 15°. It was also observed that though the error was high for lower angles they also had lower variance, as the orientation was increased; it was observed that the highest variance between measurements occurred at around 30° after which the variance reduced with increase in orientation reaching a minimum value at 75°.

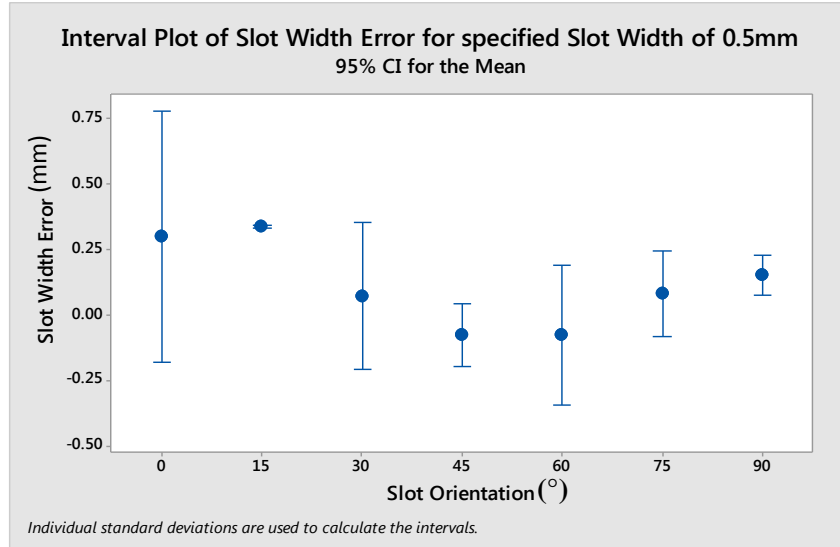


Figure 10: Interval plot of slot width error for specified slot width of 0.5mm

3.1.4 Conclusions from the Feasibility test

The first objective of the study was to determine the extent to which slot angle had on 3D printed slot width for two target slot widths of 1.0 mm and 0.5 mm. The results obtained from the feasibility test confirmed that slot width and variability in slot width does vary as a function of slot orientation. Such discrepancies are problematic with respect to 3D printing of fully functional moving assemblies, as the mating surfaces will either fuse together due to low clearance or have excessive clearance which results in a large amount of “play” between the moving parts.

3.2 Design of Experiments

A Design of Experiments (DOE) approach was used to determine the degree to which layer thickness, slot orientation and specified CAD slot width affect the measured slot width in each 3D printed sample. All experiments were performed using a MakerBot Replicator 2X 3D printer with ABS plastic (Makerbot Inc., Brooklyn, NY). The same machine was used to conduct the 36 runs (9 whole plots), and the 3D printing process parameters (e.g. temperature, extrusion speed, etc.) were kept constant throughout the experimental procedure. A new filament reel was used to conduct the DOE, in order to avoid any variation caused by moisture, for the same reason testing was done in just over two days. The default print parameters of the

MakerBot Replicator 2X were used, while only changing the 'Layer Height' for each whole plot. Figure 11 shows the default print settings used.

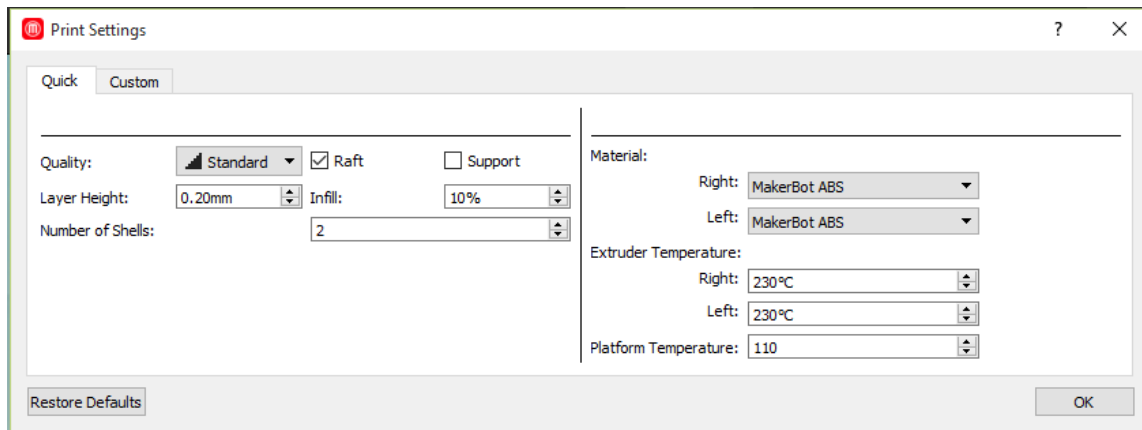


Figure 11: Print settings for design of experiment

3.2.1 Experimental Set-up

JMP statistical software was used to create a Split Plot Design having 36 runs (9 whole plots). The DOE was divided into whole plots having two hard to change factors for each whole plot - Slot Width and Layer Thickness, while the factor of Slot Angle was kept as an easy to change factor. This was done to study the effect of slot orientation while keeping the slot width and layer thickness constant for a given run. Figure 12 shows an example of the whole plots generated by the JMP software and the whole plots drafted in SolidWorks.

Whole Plot 1				Whole Plot 2			
Run Order	Slot Angle (°)	Slot Width (mm)	Layer Thickness (mm)	Run Order	Slot Angle (°)	Slot Width (mm)	Layer Thickness (mm)
1	90	1	0.3	5	30	0.75	0.1
2	0	1	0.3	6	0	0.75	0.1
3	0	1	0.3	7	60	0.75	0.1
4	90	1	0.3	8	90	0.75	0.1



Figure 12: Whole plot design

3.2.1.1 Factor Levels of Experimental Design

Three factors were considered for each experiment. Figures 13 and 14 illustrate the schematic representation of the factors considered for the experiments.

Slot Width (mm): This is the specified CAD model dimension for the slot to be printed. A 3D printed slot between two parallel surfaces is used to simulate the gap between mating surfaces in a 3D printed assembly. A series of slot widths were considered in order to determine how the printing process affects the clearance obtained between opposing surfaces when larger gaps were printed compared to when smaller gaps were printed.

Slot Orientation (°): The angle (or orientation) with respect to the build plate at which the slot is printed. The slot orientation affects the width of the 3D printed slot. A series of angles were therefore studied in the spectrum of 0 to 90 degrees to quantify the variation caused with the change of slot orientations.

Layer Thickness (mm): Layer thickness is a measure of the height of each successive addition of material in the additive manufacturing or 3D printing process in which layers are stacked.

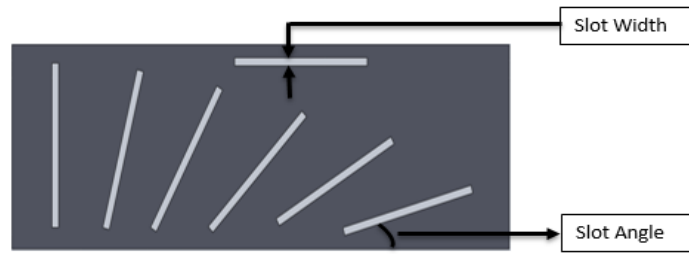


Figure 13: Slot width and slot orientation

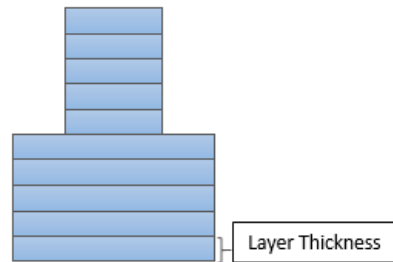


Figure 14: Layer Thickness

The slot orientation was studied at 4 levels, while the slot width and layer thickness were studied at 3 levels each. Table 4, shows the factors and levels for the DOE.

Table 4: DOE factors and levels

MAKERBOT REPLICATOR 2X DOE				
FACTOR	LEVEL			
	1	2	3	4
Slot Angle (°)	0	30	60	90
Slot Width (mm)	0.5	0.75	1	-
Layer Thickness (mm)	0.1	0.2	0.3	-

3.2.2 Evaluation and Measurement

The test pieces were printed on a MakerBot Replicator 2X. The test blocks were 125mm × 45mm × 20mm and the slots were 35mm in length. The test pieces were then placed under the Hirox 7700 microscope for image acquisition. The stitching feature of the microscope software was used to merge together multiple images into an image that contained the entire slot. The slot width was then measured for each sample. Width measurements were taken at 4 points (at 8.75mm distances starting from the top) along the length of the slot (Figure 15 and 16). This was done to obtain data across the sample and to measure the variation in the process in order to help eliminate noise. Experimental results are tabulated in Table 5.

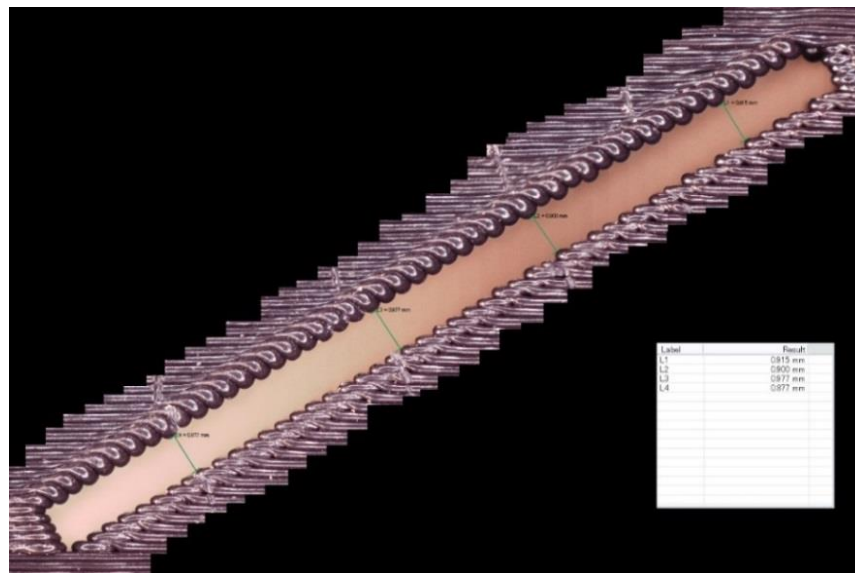


Figure 15: Slot width measurements taken at 4 points of the slot

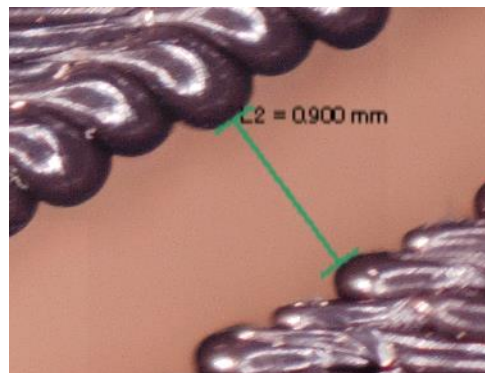


Figure 16: Enlarged view of measurements taken for DOE

Table 5: Design table and data for design of experiment (Refer Appendix)

Run Order	Whole Plot	Slot Orientation($^{\circ}$)	Slot Width (mm)	Layer Thick. (mm)	Measured Distance (mm)				Error (mm)				Avg. Error (mm)
					1	2	3	4	1	2	3	4	
1	1	90	1	0.3	0.869	0.904	0.940	1.011	0.131	0.096	0.060	-0.011	0.069
2	1	0	1	0.3	0.634	0.224	0.000	0.468	0.366	0.776	1.000	0.532	0.669
3	1	0	1	0.3	0.573	0.191	0.000	0.506	0.427	0.809	1.000	0.494	0.683
4	1	90	1	0.3	0.832	0.849	0.867	1.044	0.168	0.151	0.133	-0.044	0.102
5	2	30	0.75	0.1	0.711	0.825	0.759	0.822	0.039	-0.075	-0.009	-0.072	-0.029
6	2	0	0.75	0.1	0.278	0.140	0.000	0.000	0.472	0.610	0.750	0.750	0.646
7	2	60	0.75	0.1	0.767	0.748	0.707	0.798	-0.017	0.002	0.043	-0.048	-0.005
8	2	90	0.75	0.1	0.872	0.908	0.872	0.882	-0.122	-0.158	-0.122	-0.132	-0.134
9	3	90	0.5	0.3	0.384	0.397	0.386	0.402	0.116	0.103	0.114	0.098	0.108
10	3	0	0.5	0.3	0.293	0.000	0.245	0.378	0.207	0.500	0.255	0.122	0.271
11	3	0	0.5	0.3	0.375	0.235	0.000	0.229	0.125	0.265	0.500	0.271	0.290
12	3	90	0.5	0.3	0.423	0.397	0.432	0.400	0.077	0.103	0.068	0.100	0.087
13	4	90	1	0.1	1.073	1.120	1.120	1.130	-0.073	-0.120	-0.120	-0.130	-0.111
14	4	90	1	0.1	1.166	1.145	1.120	1.109	-0.166	-0.145	-0.120	-0.109	-0.135
15	4	0	1	0.1	0.477	0.000	0.000	0.631	0.523	1.000	1.000	0.369	0.723
16	4	60	1	0.1	1.083	1.062	1.136	1.118	-0.083	-0.062	-0.136	-0.118	-0.100
17	5	90	1	0.1	1.130	1.068	1.130	1.130	-0.130	-0.068	-0.130	-0.130	-0.115
18	5	0	1	0.1	0.615	0.114	0.000	0.315	0.385	0.886	1.000	0.685	0.739
19	5	30	1	0.1	0.931	0.984	1.015	0.882	0.069	0.016	-0.015	0.118	0.047
20	5	60	1	0.1	1.061	1.018	1.071	1.088	-0.061	-0.018	-0.071	-0.088	-0.060
21	6	0	1	0.2	0.615	0.159	0.418	0.642	0.385	0.841	0.582	0.358	0.542
22	6	0	1	0.2	0.755	0.112	0.371	0.588	0.245	0.888	0.629	0.412	0.544
23	6	90	1	0.2	0.940	0.952	0.967	0.975	0.060	0.048	0.033	0.025	0.042
24	6	30	1	0.2	0.915	0.900	0.977	0.877	0.085	0.100	0.023	0.123	0.083
25	7	60	0.75	0.3	0.740	0.721	0.767	0.753	0.010	0.029	-0.017	-0.003	0.005
26	7	0	0.75	0.3	0.410	0.240	0.000	0.186	0.340	0.510	0.750	0.564	0.541
27	7	0	0.75	0.3	0.395	0.147	0.000	0.206	0.355	0.603	0.750	0.544	0.563
28	7	90	0.75	0.3	0.619	0.650	0.650	0.762	0.131	0.100	0.100	-0.012	0.080
29	8	0	0.5	0.1	0.120	0.000	0.000	0.000	0.380	0.500	0.500	0.500	0.470
30	8	0	0.5	0.1	0.150	0.000	0.000	0.000	0.350	0.500	0.500	0.500	0.463
31	8	30	0.5	0.1	0.728	0.642	0.578	0.540	-0.228	-0.142	-0.078	-0.040	-0.122
32	8	90	0.5	0.1	0.642	0.652	0.652	0.602	-0.142	-0.152	-0.152	-0.102	-0.137
33	9	0	0.5	0.2	0.100	0.000	0.000	0.000	0.400	0.500	0.500	0.500	0.475
34	9	60	0.5	0.2	0.561	0.521	0.554	0.517	-0.061	-0.021	-0.054	-0.017	-0.038
35	9	90	0.5	0.2	0.485	0.530	0.495	0.511	0.015	-0.030	0.005	-0.011	-0.005
36	9	30	0.5	0.2	0.459	0.455	0.476	0.388	0.041	0.045	0.024	0.112	0.056

In Table 5, errors were calculated using Equation 1. A positive error indicated that the printed slot width was smaller than the specified slot width. A negative error indicated that the 3D printed slot had a dimension greater than the specified slot width. The average of the four measured values was then calculated. The average error was the response variable considered for each experiment.

3.2.3 Analysis of Results from the Design of Experiments

JMP statistical software was used to analyze the data obtained from the experiments and to formulate the analysis of variance (ANOVA). From the ANOVA in Table 6, it is clear that the factors of Slot Angle, Slot Width and Layer thickness were significant with a p-value less than 0.05. There was no strong correlation between the higher order interactions of Slot Angle + Slot Width, Slot Angle + Layer Thickness and Slot Width + Layer Thickness. It was observed the the p-value for Slot Angle was the smallest while the p-values for Slot Width and Layer Thickness were a little higher but less than 0.05. This meant that the statistical values were unlikely to be that extreme by happenstance. The conclusion drawn from the interaction effects was that even though the effects did not meet the significance criteria of being less than 0.05, this could easily be by happenstance. More data would help in providing us with a more in-depth response.

Table 6: Summary of fit and parameter Estimates

Summary of Fit

RSquare	0.589421
RSquare Adj	0.504474
Root Mean Square Error	0.161132
Mean of Response	0.202875
Observations (or Sum Wgts)	36

Parameter Estimates

Term	Estimate	Std Error	DFDen	t Ratio	Prob> t
Intercept	0.1941475	0.012221	2.818	15.89	0.0008*
Slot Angle	-0.251955	0.032772	28.41	-7.69	<.0001*
Slot Width	0.0658001	0.014236	3.02	4.62	0.0188*
Layer Thickness	0.074034	0.014221	2.982	5.21	0.0140*
Slot Angle*Slot Width	-0.033555	0.037021	29	-0.91	0.3722
Slot Angle*Layer Thickness	0.0576798	0.03645	26.73	1.58	0.1253
Slot Width*Layer Thickness	0.018398	0.017494	3.261	1.05	0.3646

Figure 17 shows that the variance is constant (homoscedasticity). As the spread seems equally distributed above and below the mean line and has a consistent spread, we can conclude the assumption of equal variance for errors is met. Also, there is no trend observed in the above graph, hence it can also be concluded the errors are independent. Figure 18 shows the histogram for the residuals. It can be observed that the data is a little skewed but follows a normal distribution overall.

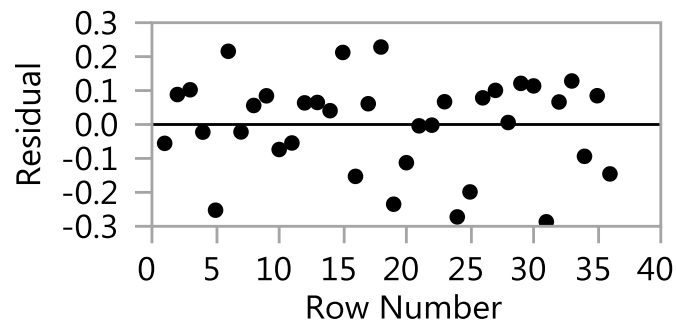


Figure 17: Row number vs residuals for error in slot width

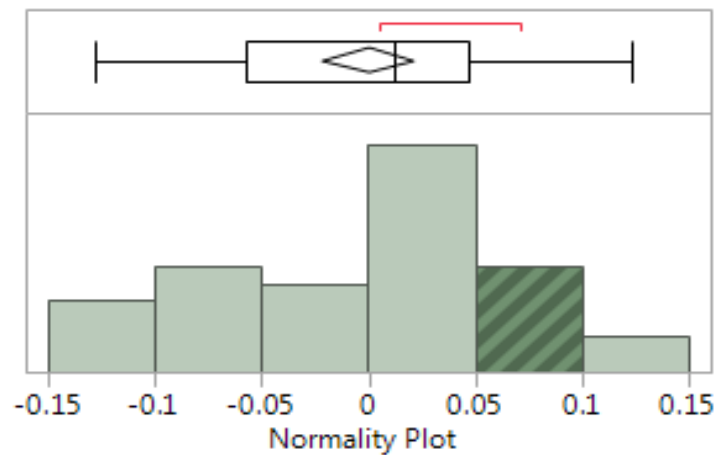


Figure 18: Normality plot for error in slot width

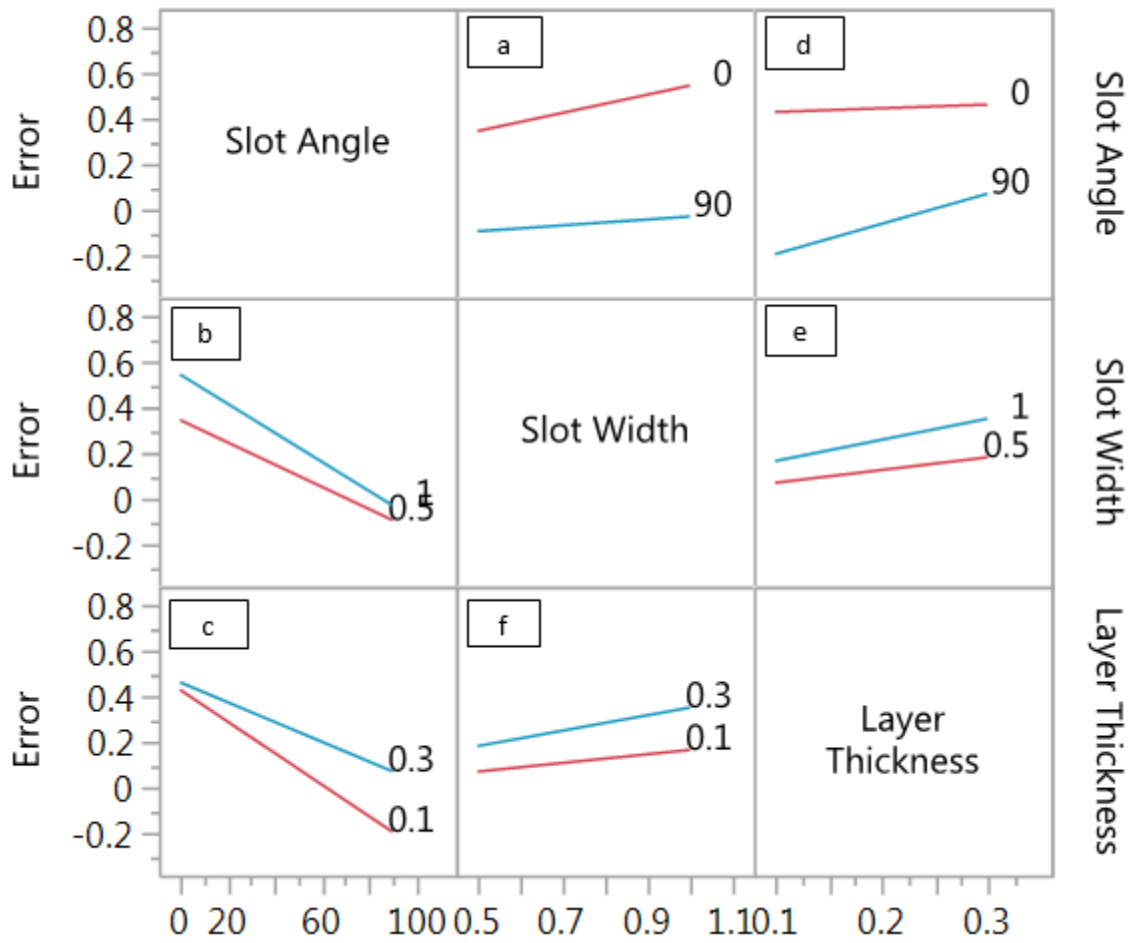


Figure 19: Interaction plot for error in slot width

From Figure 19 (b), when the slot angle is changed from 0° to 90° , the error reduces at a faster rate for the 0.5 mm wide slot compared to slot width of 1 mm. An increase in slot width with an increase in angle is therefore not necessarily a better combination.

From Figure 19 (c), when the slot angle is changed from 0° to 90° , the error for a 0.1 mm layer thickness decreases at a faster rate compared to a layer thickness of 0.3 mm. This means that as the slot angle increases from 0° to 90° , thinner layers are better. At a slot angle of 60° and a layer thickness value of 0.1 mm, the error value is closest to zero.

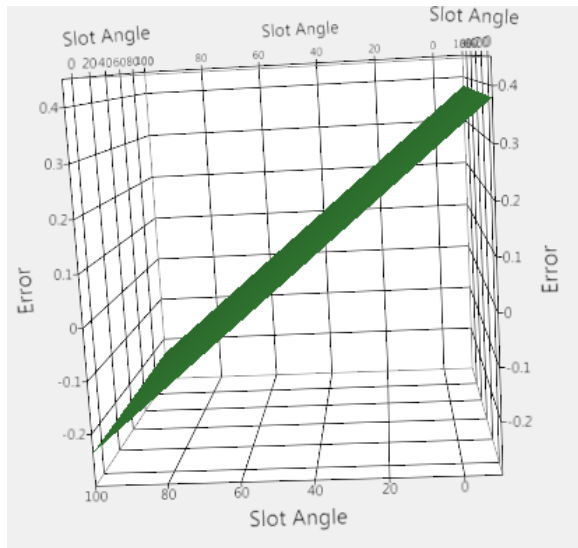
From Figure 19 (f), when the slot width increases from 0.5 mm to 1.0 mm, the error is higher for thicker layers. This means that with change in slot width from 0.5 mm to 1.0 mm, having a thinner layer produces

stable results. However, there is an error at lower levels as well but a combination of lower layer thickness and thinner slot width has a least error closest to zero.

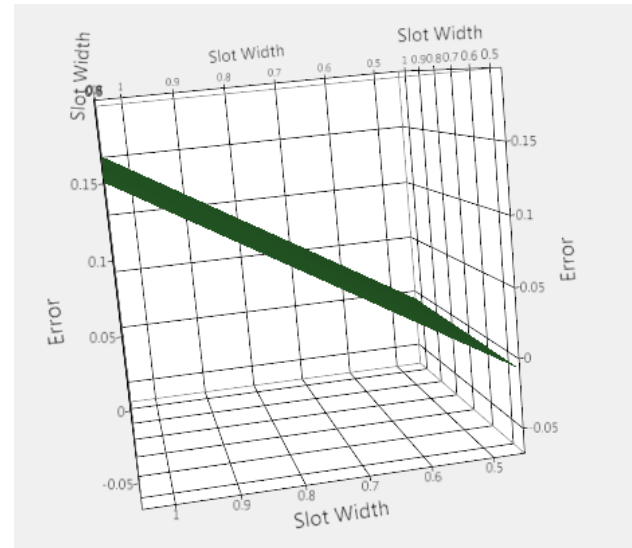
The surface plots are represented in Figure 20. Figure 20 (a) is the plot of Slot Angle vs Error. It can be observed that the print error from the nominal is highest for slot angle of 0° . As the slot angle is increased, it can be observed that the print error reduces and provides a minimum error at a slot angle of 60° . As the slot angle is further increased, it is observed that we get a negative error. It is important to note here that our optimal error value is 0, a positive error signifies that for that particular slot angle the slot width printed is smaller than the specified CAD slot width, while a negative error signifies that the slot width printed is larger than the specified CAD slot width. This observation falls in line with the observations conducted from the preliminary experiments.

Figure 20 (b), Slot Width vs Error indicates that as the slot width is increased the amount of error measured between the printed sample and the specified CAD model also increases, providing the least error at the 0.5 mm slot width.

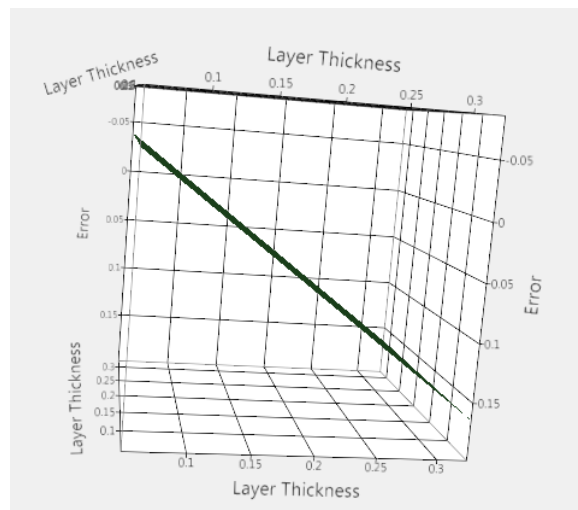
Figure 20 (c), Layer Thickness vs Error indicates that as the layer thickness is increased from 0.1 mm to 0.3 mm it is observed that the magnitude of error increases, providing the least error for a layer thickness of 0.1 mm



(a)



(b)



(c)

Figure 20: (a) Surface plot slot width error w.r.t slot angle (b) Surface plot slot width error w.r.t slot width (c) Surface plot slot width error w.r.t layer thickness

3.2.4 Conclusions from the Design of Experiments

By studying the micrographs, we could observe that as the slot angle was increased from 0° to 90° , the dimension error was caused largely due to poor surface quality of down facing surfaces. The down facing surface was the one which was being printed against gravity. For a slot angle of 0° , as there was no surface or support structure on which to print, it was observed that the error was very large. It appears that as more layers were printed, the first layer is pushed further down into the gap of the slot width thus in some cases fusing the up facing and down facing surfaces together causing the high magnitude of error. As the slot angle was increased, it was observed that the magnitude of error decreased. This was primarily due to the fact that the down facing surfaces at higher angles (i.e. 30° , 60° and 90°) were not completely against the force of gravity. The amount of overhang also reduced as the slot angle was increased.

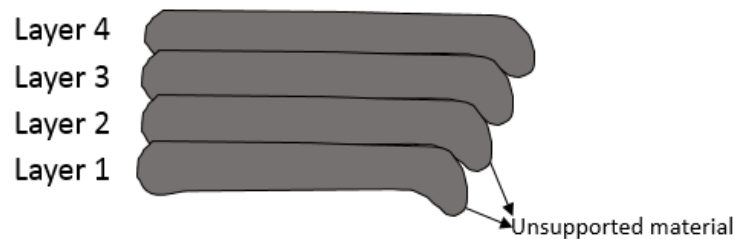


Figure 21: Diagrammatic representation of the drooping phenomenon in down facing surfaces

From the DOE analysis, it was concluded that a 60° slot angle, 0.5 mm slot width, and a 0.1 mm layer thickness provided reasonably good results. For practical applications, the slot orientation can vary depending on the application of the desired print and end use of the print. The user now has some knowledge of the process and can use this data to determine the most favorable print parameters required to print an assembly. This takes the user from relying on judgement or trial and error to using a standardized and scientific method of designing an assembly for 3D printing.

4 3D Printing a moving assembly

The experiments described in Chapter 3 studied dimensional accuracy of a gap between opposing faces in a 3D printed assembly as a function of surface orientation, layer thickness and distance between opposing surfaces. This was done in order to help validate the need for obtaining a deeper understanding of the process. The preliminary experiments along with the analysis of their results proved that there is a gap in the process which has not been studied completely. The final aim of this research was to apply insight gained from prior experimentation in order to 3D print a moving pin-hole assembly. A pin-hole assembly is one of the most commonly used assemblies in conventional manufacturing due to its simple design and wide array of applications. For this reason, the next experiment was conducted by 3D printing holes of various diameters at various angles of orientation.

4.1 3D Printed Hole Methodology

Parts with four holes having diameters of 8mm, 10mm, 12mm and 14mm respectively were designed in SolidWorks. 3D printed examples are seen in Figure 22. In the context of prior experiments, a hole has both up-facing and down-facing surfaces at every angle ranging from 0° to 90°. The aim of this experiment, therefore, was to determine how much the printed hole dimensions vary from the specified hole dimensions. Hole diameter plays a key role when assemblies are 3D printed. It was also important to study whether the magnitude of error changed as a function of hole diameter.

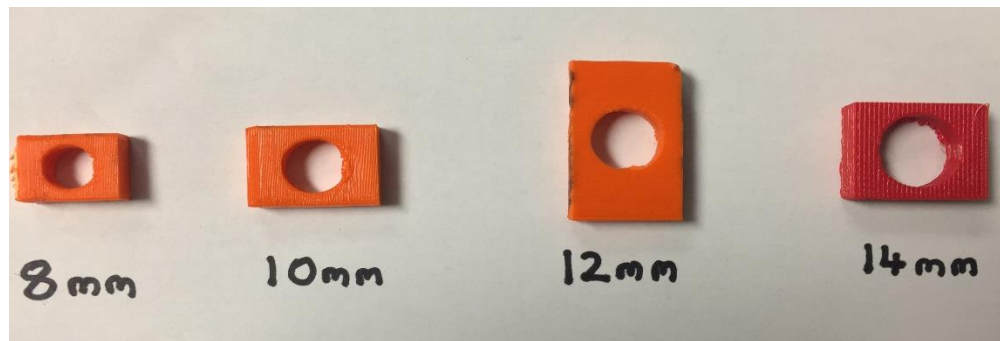


Figure 22: 3D printed holes samples

4.2 3D Printed Hole Results

For each hole of a given diameter, a sample was 3D printed in which the axis of the hole was oriented at 0°, 15°, 45°, 60°, 75°, and 90° relative to the X-Y build plane using a MakerBot Replicator 2X. ABS plastic was used with an extruder temperature of 230 C, layer thickness of 0.2 mm, and 10% infill. The minimum diameter of each hole was measured using a telescoping hole gauge and a digital caliper. The minimum hole diameter corresponds to the diameter of the largest pin that may be able to be inserted into the hole in an assembly. Three measurements were taken for each sample, and the average printed diameter was calculated (as shown in Tables 8-11). The average error was then calculated for each sample. This was done by taking the difference between the specified CAD model dimension and the average printed diameter.

Table 7 : Measured hole diameters for a nominal (specified) hole diameter of 8 mm printed at different orientations w.r.t the X-Y build plane along with the calculated relative error

Angle of Print(°)	Individual Diameter Measurements (mm)			Average Dia. (mm)	Standard Deviation	Error (mm) from specified 8 mm hole dia.	Relative Error (mm/mm)
	1	2	3				
0	7.68	7.57	7.57	7.61	0.06	0.39	0.05
15	7.41	7.25	7.49	7.38	0.12	0.62	0.08
30	7.29	7.43	7.4	7.37	0.07	0.63	0.08
45	7.44	6.28	7.12	6.95	0.60	1.05	0.13
60	7.26	7.35	7.25	7.29	0.06	0.71	0.09
75	7.24	7.23	7.23	7.23	0.01	0.77	0.10
90	7.42	7.47	7.55	7.48	0.07	0.52	0.06

Table 8: Measured hole diameters for a nominal (specified) hole diameter of 10 mm printed at different orientations w.r.t the X-Y build plane along with the calculated relative error

Angle of Print(°)	Individual Diameter Measurements (mm)			Average Dia. (mm)	Standard Deviation	Error (mm) from specified 10 mm hole dia.	Relative Error (mm/mm)
	1	2	3				
0	9.67	9.58	9.35	9.53	0.17	0.47	0.05
15	9.42	9.49	9.46	9.46	0.04	0.54	0.05
30	9.14	9.06	9.22	9.14	0.08	0.86	0.09
45	8.90	9.13	9.28	9.10	0.19	0.90	0.09
60	8.95	9.21	8.94	9.03	0.15	0.97	0.10
75	9.33	9.40	9.47	9.40	0.07	0.60	0.06
90	9.51	9.58	9.47	9.52	0.06	0.48	0.05

Table 9: Measured hole diameters for a nominal (specified) hole diameter of 12 mm printed at different orientations w.r.t the X-Y build plane along with the calculated relative error

Angle of Print(°)	Individual Diameter Measurements (mm)			Average Dia. (mm)	Standard Deviation	Error (mm) from specified 12 mm hole dia.	Relative Error (mm/mm)
	1	2	3				
0	11.47	11.62	11.52	11.54	0.08	0.46	0.04
15	11.16	11.1	11.49	11.25	0.21	0.75	0.06
30	11.27	11.28	11.30	11.28	0.02	0.72	0.06
45	11.39	11.53	11.38	11.43	0.08	0.57	0.05
60	11.46	11.54	11.50	11.50	0.04	0.50	0.04
75	11.62	11.83	11.48	11.64	0.18	0.36	0.03
90	11.72	11.6	11.51	11.61	0.11	0.39	0.03

Table 10: Measured hole diameters for a nominal (specified) hole diameter of 14 mm printed at different orientations w.r.t the X-Y build plane along with the calculated relative error

Angle of Print(°)	Individual Diameter Measurements (mm)			Average Dia. (mm)	Standard Deviation	Error (mm) from specified 14 mm hole dia.	Relative Error (mm/mm)
	1	2	3				
0	13.49	13.49	13.50	13.49	0.01	0.51	0.04
15	13.35	13.25	13.41	13.34	0.08	0.66	0.05
30	13.31	13.27	13.20	13.26	0.06	0.74	0.05
45	13.20	13.08	13.19	13.16	0.07	0.84	0.06
60	12.82	13.10	13.13	13.02	0.17	0.98	0.07
75	12.84	13.17	13.15	13.05	0.19	0.95	0.07
90	13.45	13.34	13.42	13.40	0.06	0.60	0.04

The relative error in Tables 7-10 was calculated using the equation:-

$$Relative\ Error = \frac{Measured\ Error}{Specified\ CAD\ model\ dimension} \quad (2)$$

The relative error was calculated to determine if there was a correlation between the error and the diameter of the printed hole. Figure 23 shows the relative error and the angle of orientation was plotted. Careful study of the graph suggests that although the hole orientation appears to have little effect on relative error, the smaller hole diameters appeared to have somewhat larger relative error than the larger holes.

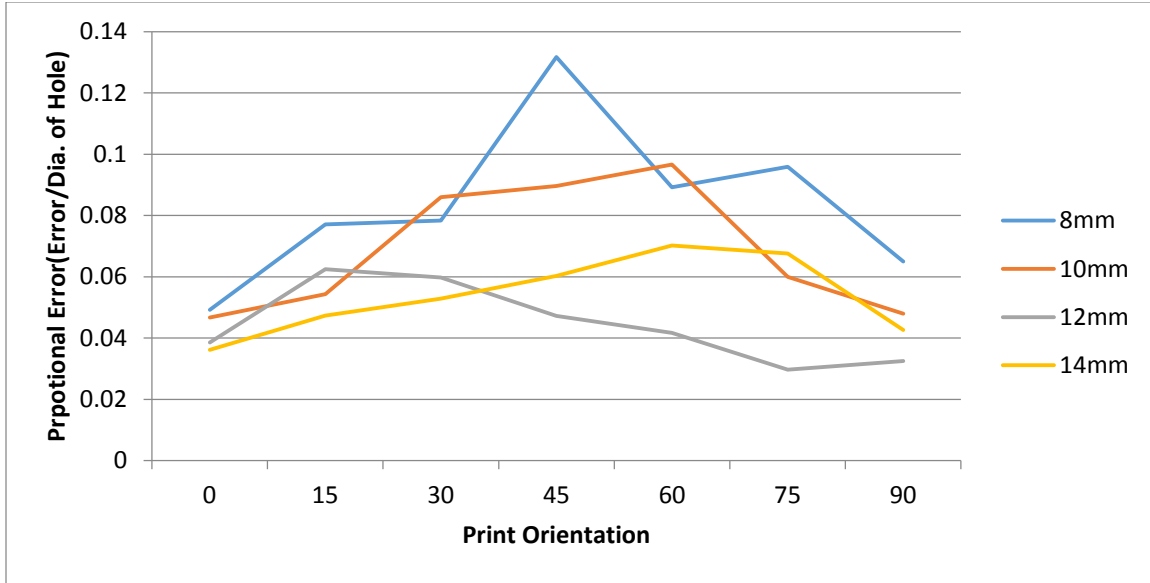


Figure 23: Relative error measured for 3D printed hole

4.3 3D Printed Hole Conclusions

The 3D printed hole experiments showed that the variability between the specified dimension and the printed dimension was very high. The process was looked into more closely, and it was observed that 3D printed holes all have concave down-facing sections which are printed against gravity. When these down-facing sections are printed, the unsupported extruded plastic has a tendency to sag from its original shape. As more layers are deposited on this unsupported concave contour, the cylindrical surface deforms to a shape that resembles an ellipse. It was concluded that due to the sagging phenomenon and the inherent variability in the process, it would be difficult to get standard results on a consistent basis. An alternative approach to 3D printing of pin-hole assemblies was therefore sought.

4.4 3D Printed Polygonal Hole-Pin Features

Results from the 3D printed hole tests revealed challenges pertaining to sagging of the down-facing region of each hole. As an alternative, the use of polygonal, rather than a cylindrical, holes was studied. Using polygonal holes is an intriguing concept, as it allows one to inscribe a cylindrical hole inside the polygonal hole. Figure 24 shows three variations of assemblies that can be 3D printed, the three figures have the exact pin diameter and the same minimum CAD clearance between the pin and hole. Figure 24 (a) shows the

conventional approach of printing a simple pin-hole assembly, where the pin and the hole are cylindrical in shape. When the model is sliced in the unconventional approach, the software generates the slices as line segments in a plan and thus does not require to generate line segments as circular interpolations as is the case with the conventional approach. Therefore when the conventional pin-hole assembly is 3D printed, the down facing concave sections are printed under gravity and have the tendency to sag from their original shape and hence are likelier to fuse with the mating surface. Due to the above reasons, it was sought to apply an unconventional approach to overcome the drawbacks of the conventional pin-hole assembly. The unconventional approach consisted of using a cylindrical pin-hexagonal hole assembly. There are several ways the assembly could have been printed, shown in Figures 24 (b) and 23 (c). The primary difference between Figures (b) and (c) is that hexagonal hole in Figure (b) would be printed at a 30° angle to the build plate whereas in Figure (c), it would be printed parallel or horizontal to the build plate. It was decided to use the Figure (b) approach, wherein the hexagonal hole will be printed at a 30° angle to the build plate. As it was seen from earlier experiments, a horizontal or parallel contour will be unsupported and though it follows a linear contour it will tend to sag thus having a higher chance of fusing with its mating surface. Secondly, where the filament would be pulled into the hole-pin clearance area in the pin-hole assembly causing the mating surfaces to fuse is where in the pin-hexagon assembly we get the maximum clearance, which is in the corners. Therefore even though both the assemblies (i.e. the pin-hole and hexagonal pin-hole) have the same specified CAD clearance, the hexagonal pin-hole assembly provides with the additional clearance in the corners. Thus having a less likely chance of the mating surfaces fusing.

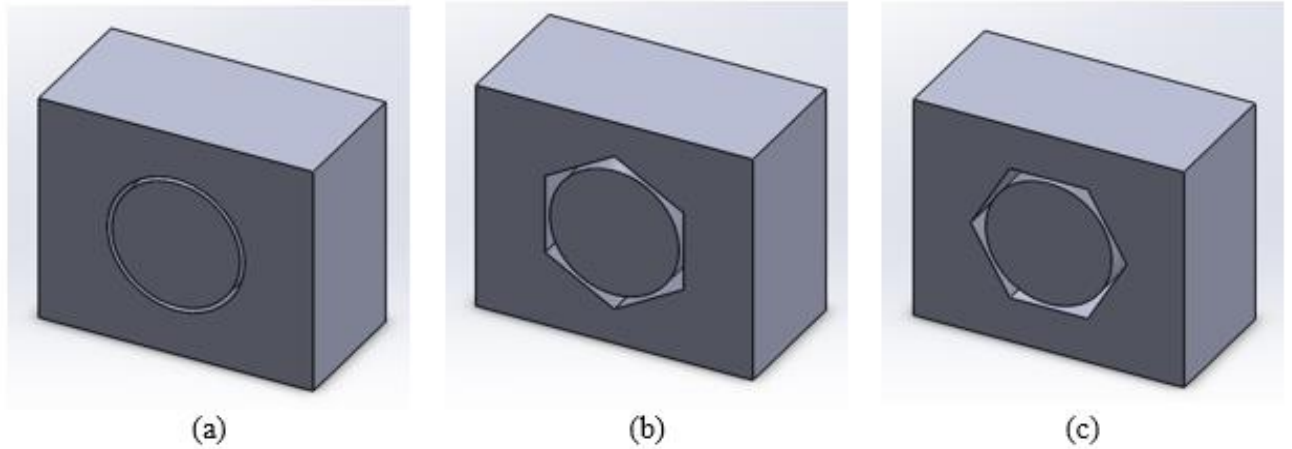


Figure 24: (a) Conventional approach for a pin-hole assembly; (b) Unconventional approach for a pin-hole assembly where hexagonal hole is at a 30° to the build plate; (c) Unconventional approach for a pin-hole assembly where hexagonal hole is at a parallel to the build plate

In order to experimentally test whether or not a hexagonal hole-pin feature is more effective than a cylindrical hole-pin feature, another set of experiments were conducted. Specifically, sets of 3D printed hexagonal hole-pin assemblies were 3D printed at different pin axis orientations and pin-hole clearances. As a baseline for comparison, a set of conventional hole-pin assemblies were produced in the same print as the hexagonal hole-pin assemblies.

The assemblies were 3D printed in ABS plastic on a MakerBot Replicator 2X with a nozzle temperature of 230°C , a build plate temperature of 110°C , and a layer thickness of 0.2mm. The samples were printed at different orientations such that the axis of the pins were at angles of 0° , 30° , 60° and 90° with respect to the build plate. All process parameters were kept constant for all the prints. Due to the build orientation, automatically generated support structures were inserted by the slicing software to hold the pin in place during the print. A preview of the build platform showing the assemblies in four different orientations plus the support structure is seen in Figure 25.

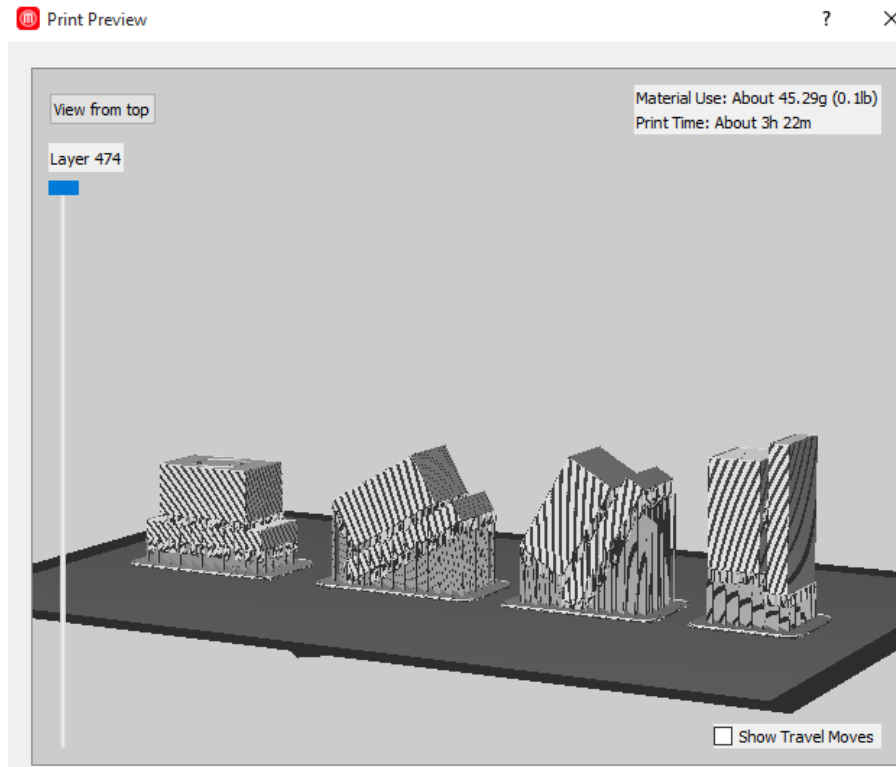


Figure 25: Print preview in of the build platform showing assemblies in four different orientations along with support structures

Once the samples were printed, the support structure was removed by applying slight twisting pressure to the cylindrical pin in the hexagonal hole-pin assembly. The cylindrical pin was separated from the hexagonal hole, and rotary motion of the pin in the hexagonal hole was thus obtained.

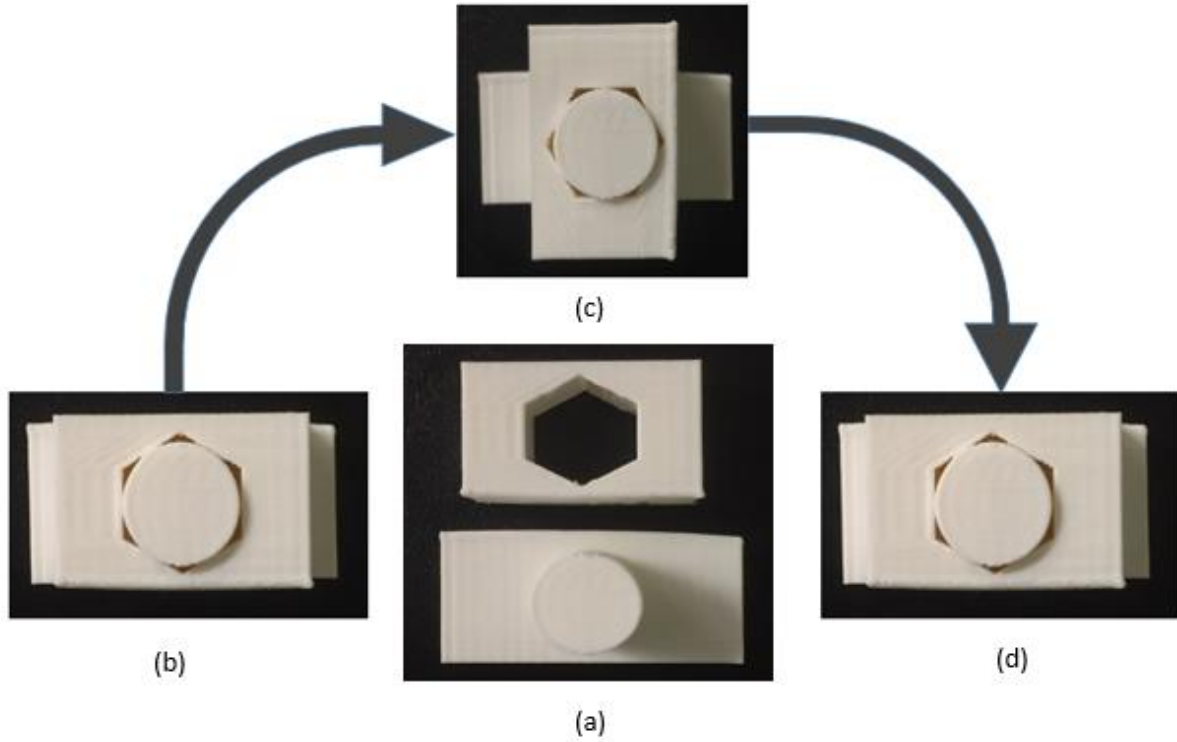


Figure 26: Moving cylindrical pin-hexagon hole assembly

Figure 26 demonstrates the moving assembly. Figure 26(a) shows the pin-hole assembly after components have been completely separated from each other. Figure 26(b) shows the pin-hexagon assembly at 0° , Figure 26(c) shows the assembly once it is rotated 90° and finally Figure 26(d) shows the assembly at a position at 180° once it is rotated again. Thus successfully demonstrating a 3D printed moving assembly.

When the same method was applied to the cylindrical hole-pin assembly, it was observed that the pin had fused with the hole, thus making a moving assembly infeasible. Figure 27 shows a cylindrical hole-pin assembly which has fused.



Figure 27: Fused cylindrical pin- cylindrical hole assembly

Tables 11 and 12 show results obtained from the validation experiments. A value of 1 indicates that a moving 3D printed assembly was successfully produced, and a value of 0 indicates that the assembly fused together and the print was unsuccessful.

Table 11 shows that 11 out of 12 hexagonal hole-pin assemblies i.e. 91% of test samples were successfully printed. The print at 13.6mm at 30° was unsuccessful. When these results were compared to 3D printed cylindrical hole-pin assemblies (Table 12), it was found that only 3 out of 12 cylindrical hole-pin assemblies i.e. only 25% of test samples were successfully produced. These three prints had the maximum hole-pin clearance of 0.5 mm, while the prints having a clearance of 0.25 mm and 0.2 mm failed completely. From this, it can be concluded that this new approach to producing hole-pin assemblies using hexagonal holes rather than cylindrical holes yields better results.

Table 11: Dimensions used to print the hexagonal hole-cylindrical pin validation assembly

Pin Dia. (mm)	Hexagon Inscribed Circle Dia. (mm)	Min. Hex/Pin Clearance (mm)	Pin Axis Orientation (degrees)			
			0	30	60	90
14.00	13.00	0.50	1	1	1	1
14.00	13.50	0.25	1	1	1	1
14.00	13.60	0.20	1	0	1	1

Table 12: Dimensions used to print the cylindrical hole-cylindrical pin validation assembly

Pin Dia. (mm)	Hole Dia. (mm)	Hole/Pin Clearance (mm)	Pin Axis Orientation (degrees)			
			0	30	60	90
14.00	13.00	0.50	0	1	1	1
14.00	13.50	0.25	0	0	0	0
14.00	13.60	0.20	0	0	0	0

5 Conclusions and Recommendations for Future Research

5.1 Summary

The primary focus of this work was to gain a better understanding of parameters leading to success or failure of 3D printed assemblies produced using the FFE process. The success or failure of a printed assembly is largely determined by the amount of clearance between mating surfaces, as well as process parameters such as surface orientation and layer thickness. When the 3D printed gap between mating surfaces is substantially smaller than the CAD model clearance, it results in a failed attempt to 3D print a moving assembly. From the experiments performed, it was concluded that the three factors, slot orientation, slot width and layer thickness had a significant effect on printed clearance along with the interaction effects between. From the design of experiments, it was observed that as the slot orientation was increased from 0° to 90° the magnitude of error between the printed sample and specified CAD model reduced and reach a minimum error value closest to 0 at the 60° slot angle. Careful study of the micrographs and data showed that at a 0° slot angle, the downward facing surface of the slot width is unsupported and under the influence of gravity, this causes the layers to sag causing the two mating surfaces to fuse. It was also observed that the least error was obtained for a slot width of 0.5 mm and a layer thickness of 0.1 mm. Hence it was concluded that a slot angle of 60° , a slot width of 0.5 mm and a layer thickness of 0.1 mm result in the least error.

In addition to developing a better understanding of process parameters that affect printed clearances between mating parts, another aim of this work was to successfully print a hole-pin moving assembly. Cylindrical hole samples were printed, and it was observed that the unsupported down-facing portion of each hole loses its shape and produces a slightly elliptical out-of-round shape. This observation led to a new unconventional method of 3D printing moving hole-pin assembly features.

It was decided to use a polygonal hole-pin assembly feature rather than a cylindrical hole-pin assembly feature. The polygonal hole geometry overcame the drawbacks of the pin-hole assembly which were:

- 1) The horizontal down-facing “ceiling” of holes slumps against gravity as the material is extruded.
- 2) Infinite points of contact between a cylindrical hole and pin increases the chances of the two surfaces fusing together.

The printed samples corroborated the assumptions of the advantage of the hexagonal hole-pin assembly over the cylindrical hole-pin assembly. Based on the results of the validation experiment, it is suggested that users should use the hexagonal hole-pin assembly approach over the cylindrical hole-pin assembly approach for 3D printing applications for consistent results.

5.2 Recommendations for Future Work

In this research, a DOE was performed using the Fused Filament Extrusion (FFE) approach on a MakerBot Replicator 2X 3D printer. However, the FDM/FFE process is fundamentally different from other 3D printing processes such as stereolithography, selective laser sintering, etc. It would be worthwhile to extend the study to other 3D printing processes on which printed assemblies are of interest.

The novel portion of this research using polygonal holes was experimentally validated using hexagonal hole-pin assembly. It would be interesting to further the research and determine the optimal number of sides or side length of a polygon to 3D print assemblies. The number of polygon sides affects the number of contact points between the pin and hole, and it also affects the orientation of down-facing printed surfaces. It is also suggested that a study be done by using an equilateral triangle inscribed in a circle instead of a hexagon. Once consistent results are established, future work should also include developing an optimization algorithm which takes into account the printing error and compensates for the printing error in the CAD file.

It would be interesting to study how the printer position resolution affects the dimensions of the printed slot width. As the MakerBot Replicator 2X uses a belt and pulley mechanism, it will be interesting to either use pulleys of smaller diameter to improve print resolution or designing the part such that the slot width is a

multiple of the printer position resolution. The printer position resolution can be calculated by using the equation:-

$$\text{Printer position resolution } \left(\frac{\text{mm}}{\text{step}} \right) = \frac{\pi D}{\text{number of steps per revolution}} \quad (3)$$

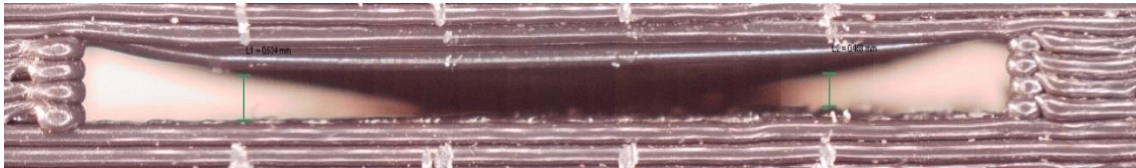
Therefore, for example if the pulley diameter is (D) 12.7 mm and the number of steps per revolution is 200, the printer position resolution will be 0.199 mm/step. This phenomenon may be a significant source of error.

6 References

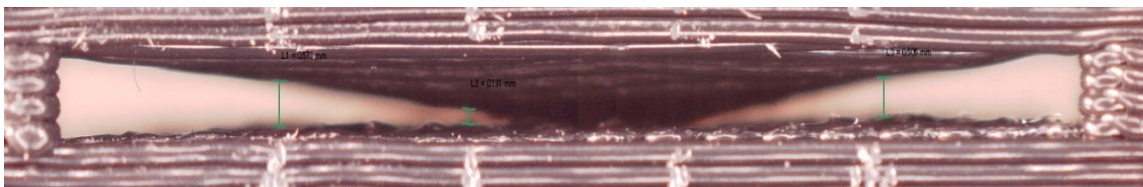
- [1] G. N. Levy, R. Schindel, and J.-P. Kruth, "Rapid manufacturing and rapid tooling with layer manufacturing (LM) technologies, state of the art and future perspectives," *CIRP Annals-Manufacturing Technology*, vol. 52, pp. 589-609, 2003.
- [2] S. Rajagopalan and M. R. Cutkosky, "Tolerance representation for mechanism assemblies in layered manufacturing," in *Proceedings of the 1998 ASME DETC/DFM Conference*, 1998, pp. 13-16.
- [3] E. Palermo, "Fused Deposition Modeling: Most Common 3D Printing Method," 2015. Available: <http://www.livescience.com/39810-fused-deposition-modeling.html>
- [4] (2015, *Fused Deposition Modeling (FDM)*); <http://www.custompartnet.com/wu/fused-deposition-modeling>. Available: <http://www.custompartnet.com/wu/fused-deposition-modeling>
- [5] M. Eragubi. (2015, *Slicing 3D CAD Model in STL Format and Laser Path Generation*," *International Journal of Innovation, Management and Technology* vol. 4, no. 4, pp. 410-413, 2013. Available: <http://www.ijimt.org/papers/431-M1007.pdf>
- [6] M. Armbruster, "3D Printing: Understanding Support Material," 2015. Available: <http://www.pddnet.com/blog/2012/07/3d-printing-understanding-support-material>
- [7] S. S. Crump, J. W. Comb, W. R. Priedeman Jr, and R. L. Zinniel, "Process of support removal for fused deposition modeling," ed: Google Patents, 1996.
- [8] R. Arni and S. Gupta, "Manufacturability analysis of flatness tolerances in solid freeform fabrication," *TRANSACTIONS-AMERICAN SOCIETY OF MECHANICAL ENGINEERS JOURNAL OF MECHANICAL DESIGN*, vol. 123, pp. 148-156, 2001.
- [9] R. Paul and S. Anand, "Optimal part orientation in Rapid Manufacturing process for achieving geometric tolerances," *Journal of Manufacturing Systems*, vol. 30, pp. 214-222, 2011.

- [10] R. Ippolito, L. Iuliano, and A. Gatto, "Benchmarking of rapid prototyping techniques in terms of dimensional accuracy and surface finish," 1995.
- [11] L. Galantucci, F. Lavecchia, and G. Percoco, "Experimental study aiming to enhance the surface finish of fused deposition modeled parts," *CIRP Annals-Manufacturing Technology*, vol. 58, pp. 189-192, 2009.
- [12] R. Paul and S. Anand, "Optimization of layered manufacturing process for reducing form errors with minimal support structures," *Journal of Manufacturing Systems*, 2014.
- [13] C. Relvas, A. Ramos, A. Completo, and J. A. Simões, "A systematic approach for an accuracy level using rapid prototyping technologies," *Proceedings of the Institution of Mechanical Engineers, Part B: Journal of Engineering Manufacture*, vol. 226, pp. 2023-2034, 2012.
- [14] R. I. Campbell, M. Martorelli, and H. S. Lee, "Surface roughness visualisation for rapid prototyping models," *Computer-Aided Design*, vol. 34, pp. 717-725, 2002.
- [15] G. Krolczyk, P. Raos, and S. Legutko, "Experimental analysis of surface roughness and surface texture of machined and fused deposition modelled parts," *Tehnički Vjesnik-Technical Gazette*, vol. 21, pp. 217-221, 2014.
- [16] D. Dimitrov, K. Schreve, and N. De Beer, "Advances in three dimensional printing-state of the art and future perspectives," *Journal for New Generation Sciences*, vol. 4, pp. p. 21-49, 2006.
- [17] J. Kietzman, "Rapid prototyping polymer parts via shape deposition manufacturing," Stanford University, 1999.
- [18] I. Fidan, "Bench marking studies for 3D printing process," *1st Annual Manufacturing Technology Summit*, p. 2, 2004.
- [19] B. Vayre, F. Vignat, and F. Villeneuve, "Designing for additive manufacturing," *Procedia CIRP*, vol. 3, pp. 632-637, 2012.

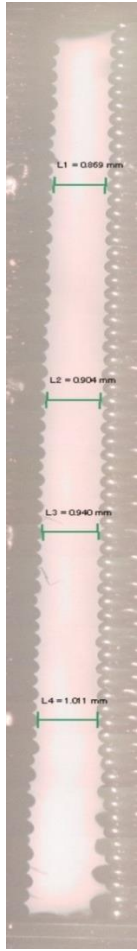
7 Appendix: Micrographs for Design of Experiments



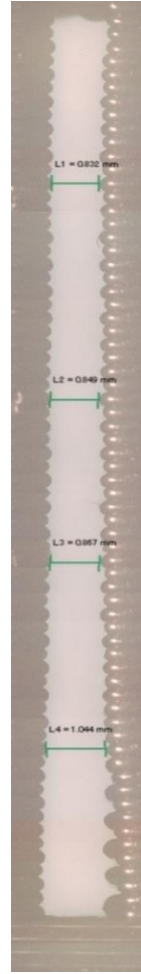
Run order 1: Slot Angle of 0°



Run order 2: Slot Angle of 0°



Run order 3: Slot Angle of 90°

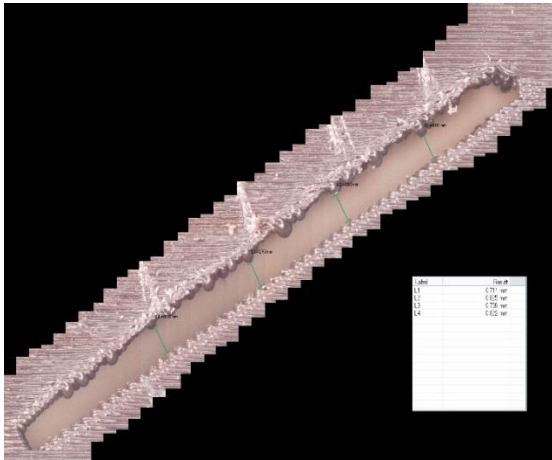


Run order 4: Slot Angle of 90°

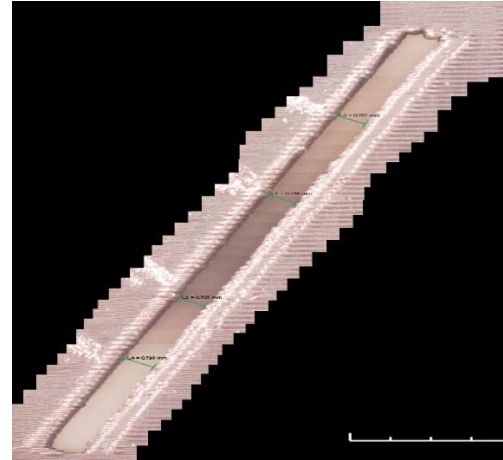
Figure 28: Whole Plot 1



Run order 5: Slot Angle of 0°



Run order 6: Slot Angle of 30°

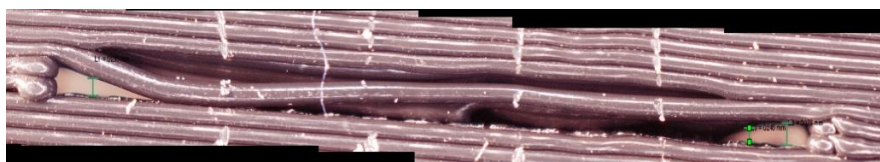


Run order 7: Slot Angle of 60°

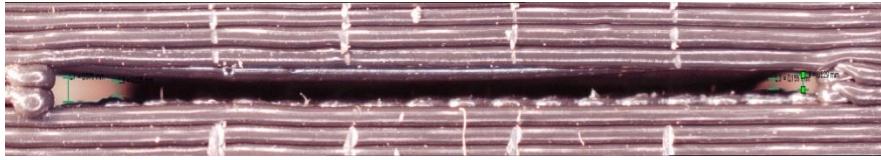


Run order 8: Slot Angle of 60°

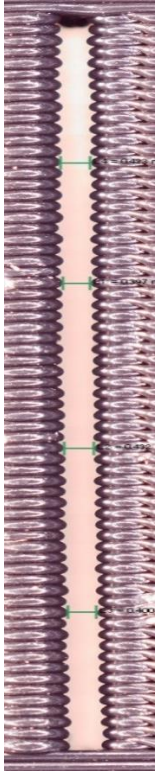
Figure 29: Whole Plot 2



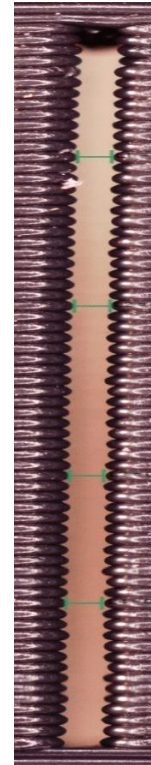
Run order 9: Slot Angle of 0°



Run order 10: Slot Angle of 0°

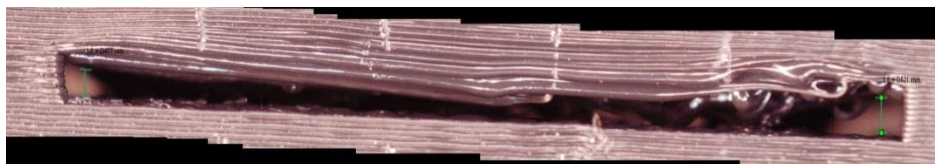


Run order 11: Slot Angle of 90°

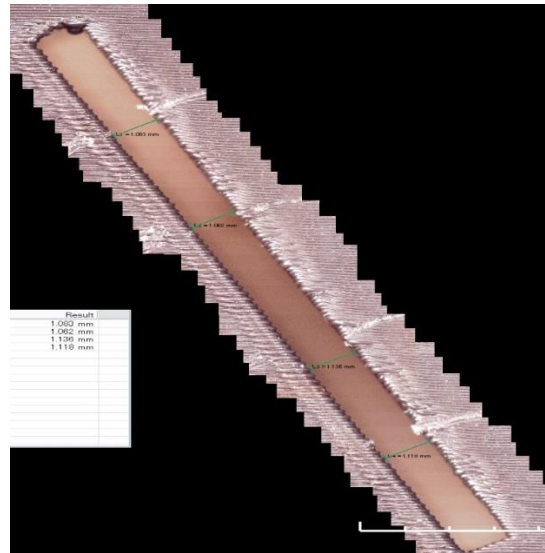


Run order 12: Slot Angle of 90°

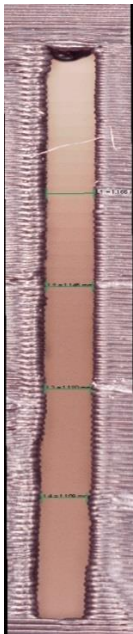
Figure 30: Whole Plot 3



Run order 13: Slot Angle of 0°



Run order 14: Slot Angle of 60°

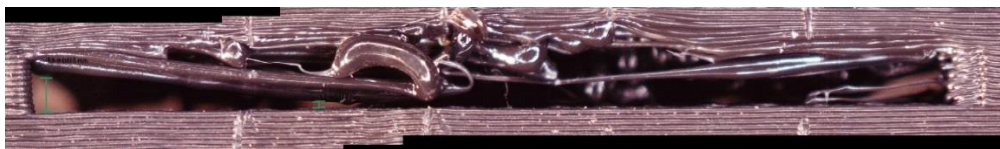


Run order 15: Slot Angle of 90°

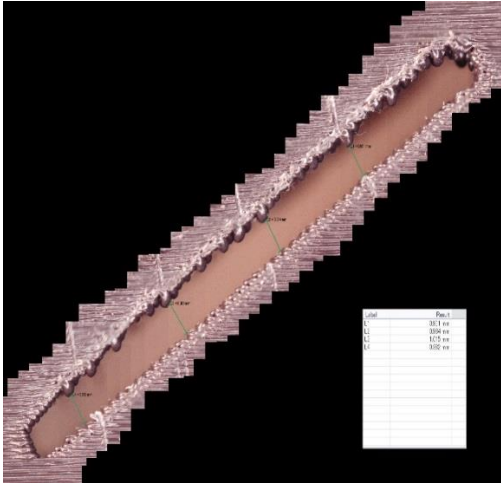


Run order 16: Slot Angle of 90°

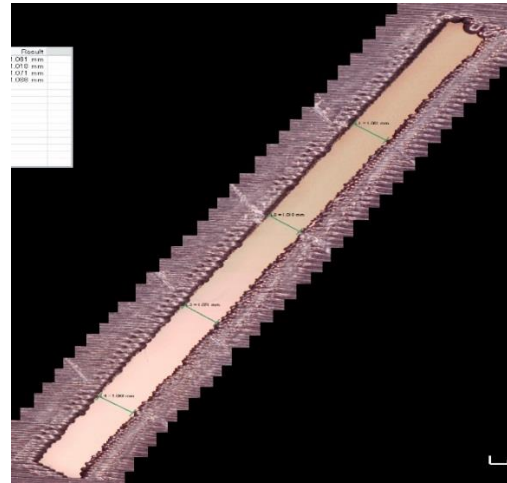
Figure 31: Whole Plot 4



Run order 17: Slot Angle of 0°



Run order 18: Slot Angle of 30°

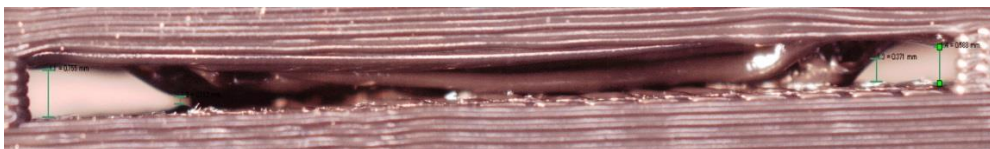


Run order 19: Slot Angle of 60°

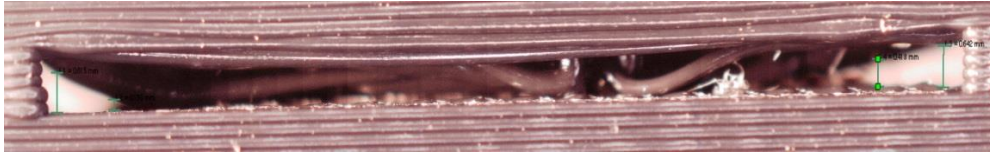


Run order 20: Slot Angle of 90°

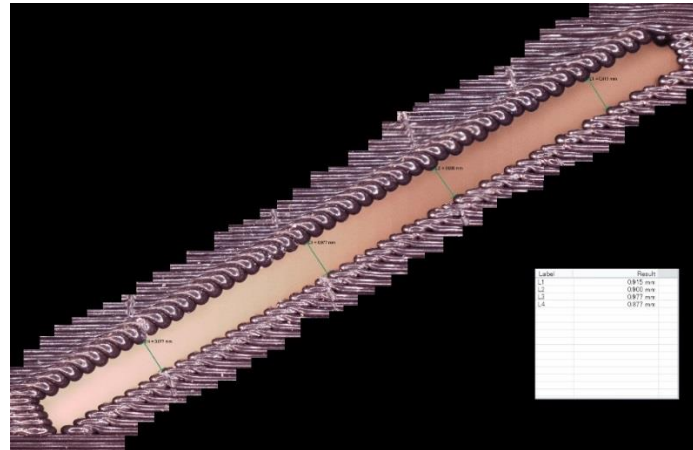
Figure 32: Whole Plot 5



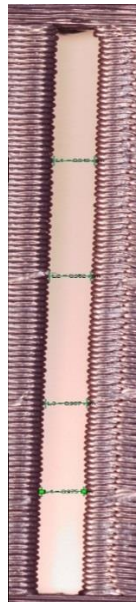
Run order 21: Slot Angle of 0°



Run order 22: Slot Angle of 0°



Run order 23: Slot Angle of 30°

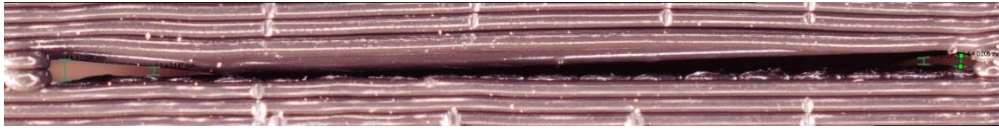


Run order 24: Slot Angle of 30°

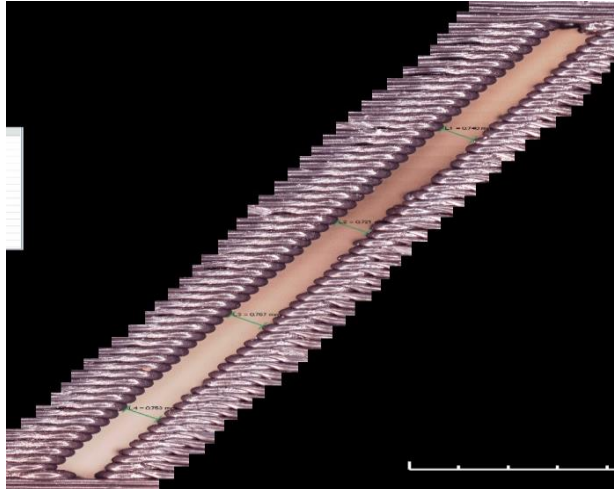
Figure 33: Whole Plot 6



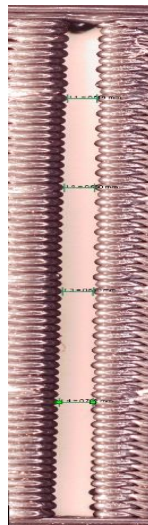
Run order 25: Slot Angle of 0°



Run order 26: Slot Angle of 0°

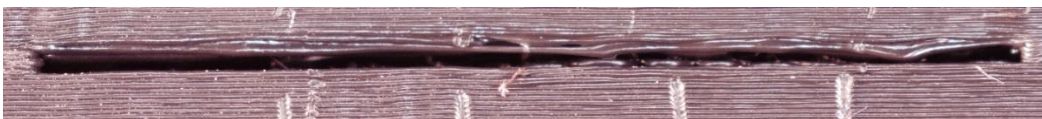


Run order 27: Slot Angle of 60°



Run order 28: Slot Angle of 30°

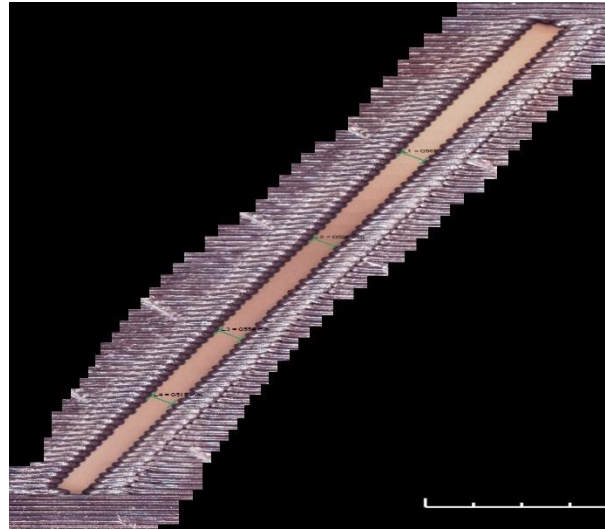
Figure 34: Whole Plot 7



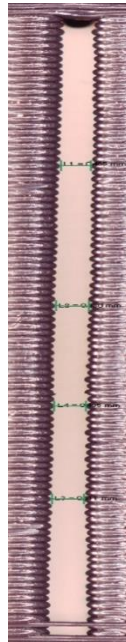
Run order 29: Slot Angle of 0°



Run order 34: Slot Angle of 30°



Run order 35: Slot Angle of 60°



Run order 36: Slot Angle of 90°

Figure 36: Whole Plot 9